Article

Multiobjective Optimization of a Hybrid PV/Wind/Battery/Diesel Generator System Integrated in Microgrid: A Case Study in Djelfa, Algeria

Zakaria Belboul [1], **Belgacem Toual** [1], **Abdellah Kouzou** [1,2,3,*], **Lakhdar Mokrani** [4], **Abderrahman Bensalem** [1], **Ralph Kennel** [3] and **Mohamed Abdelrahem** [3,5,*]

1 Laboratory of Applied Automation and Industrial Diagnostics (LAADI), Faculty of Science and Technology, Ziane Achour University, Djelfa 17000, Algeria; z.belboul@univ-djelfa.dz (Z.B.); toualb@gmail.com (B.T.); ab.bensalem@univ-djelfa.dz (A.B.)
2 Electrical and Electronics Engineering Department, Nisantasi University, Istanbul 34398, Turkey
3 Institute for High-Power Converter Systems (HLU), Technical University of Munich (TUM), 80333 Munich, Germany; ralph.kennel@tum.de
4 LACoSERE Laboratory, Department of Electrical Engineering, Faculty of Technology, University Amar Telidji of Laghouat, Laghouat 03000, Algeria; mokrani_lakhdar@hotmail.com
5 Department of Electrical Engineering, Assiut University, Assiut 71516, Egypt
* Correspondence: kouzouabdellah@ieee.org (A.K.); mohamed.abdelrahem@tum.de (M.A.)

Abstract: Hybrid Renewable Energy Sources (HRES) integrated into a microgrid (MG) are a cost-effective and convenient solution to supply energy to off-grid and rural areas in developing countries. This research paper focuses on the optimization of an HRES connected to a stand-alone microgrid system consisting of photovoltaics (PV), wind turbines (WT), batteries (BT), diesel generators (DG), and inverters to meet the energy demand of fifteen residential housing units in the city of Djelfa, Algeria. In this context, the multiobjective salp swarm algorithm (MOSSA), which is among the latest nature-inspired metaheuristic algorithms recently introduced for hybrid microgrid system (HMS) optimization, has been proposed in this paper for solving the optimization of an isolated HRES. The proposed multiobjective optimization problem takes into account the cost of energy (COE) and loss of power supply probability (LPSP) as objective functions. The proposed approach is applied to determine three design variables, which are the nominal power of photovoltaic, the number of wind turbines, and the number of battery autonomy days considering higher reliability and minimum COE. In order to perform the optimum size of HMG, MOSSA is combined with a rule-based energy management strategy (EMS). The role of EMS is the coordination of the energy flow between different system components. The effectiveness of using MOSSA in addressing the optimization issue is investigated by comparing its performance with that of the multiobjective dragonfly algorithm (MODA), multiobjective grasshopper optimization algorithm (MOGOA), and multiobjective ant lion optimizer (MOALO). The MATLAB environment is used to simulate HMS. Simulation results confirm that MOSSA achieves the optimum system size as it contributed 0.255 USD/kW h of COE and LPSP of 27.079% compared to MODA, MOGOA, and MOALO. In addition, the optimization results obtained using the proposed method provided a set of design solutions for the HMS, which will help designers select the optimal solution for the HMS.

Keywords: multiobjective salp swarm algorithm; solar energy; microgrid; energy management strategy; batteries; wind; Djelfa

1. Introduction

Population increase, rising energy consumption, rising energy production costs, greenhouse gas emissions, and damage caused by fossil resources to the environment have led to a greater emphasis on renewable energy sources [1–4].

Although there have been considerable increases in renewable energy technology, electricity shortages remain a problem in rural communities and islands. According to the United Nations Development Program (UNDP), more than a quarter of the world's population, particularly those living in rural regions, suffer from lack of access to electricity. Rural communities are typically isolated from the national grid and situated in challenging terrain, such as steep terrain or dense jungle, making transmission line extension prohibitively expensive or impossible. Renewable resources, such as wind, solar, and hydropower, help these areas save energy because they possess potentially ubiquitous, abundant, accessible, clean, and easy-to-obtain energy [5,6].

The most accessible and critical renewable resources, wind and solar energy, are combined to create a higher quality and more reliable hybrid energy system than individual resources [1–4]. In fact, in a hybrid energy system, wind and solar energy are the primary energy sources. Battery units, energy storage, fuel cells, and DGs can all be used in hybrid systems to improve efficiency and eliminate flaws. Indeed, when wind speed or solar radiation falls below a certain threshold or when a peak in demand arises, the presence of these storage devices becomes critical [4,7,8].

Renewable energy in the form of an HMS System is the most efficient, dependable, and cost-effective way to use localized renewable energy resources which combine renewable energy sources with a diesel generator as a backup system to provide centralized electricity generation at the local level. These systems range in size from a basic 5 kW single-phase system for a single residence to a massive three-phase network that serves as a primary power supply for the entire neighborhood. When demand grows or the community expands, they can quickly scale up and connect to the national grid [6,9].

Microgrid systems based on autonomous renewable energy sources (RES) are the most viable and cost-effective option for electrifying off-grid areas [10,11]. Therefore, from an economic and technical standpoint, such a system's planning and optimal design are complex for various reasons. One of these reasons would be the inconsistency of RESs and their reliance on meteorological conditions. Microgrid systems are frequently either over- or undersized in order to meet energy demand. An oversized system will have a high operating cost and will create extra energy. Conversely, an undersized microgrid system will fail to supply electricity to the required loads. To fully realize the benefits of an RES-based microgrid, optimum microgrid sizing combined with a robust energy management strategy is required [11,12].

1.1. Literature State of the Art

A large number of works has been reported in the field of hybrid microgrid system sizing. Previous methodologies in the area of sizing can be grouped into different categories [13–16]. The first category—software tools such as HOMER, HOMER Pro, PVSYST, HOGA, IHOGA, and RAPSIM—was applied to optimize microgrid systems [17–23]. Despite being simple to use, this category has the drawback of users being unable to select appropriate system components intuitively. Furthermore, users have no access to or visibility of the calculations and algorithms [19,24]. The second category contains deterministic methods such as iterative, analytical, numerical, graphical construction, etc. [25–31]. Although simple, these methods require considerable simulation time, as all system configurations are analyzed [26]. The third category includes metaheuristic algorithms for solving microgrid problems, many of which have been utilized in the literature to tackle optimization problems where authors [32] developed a recent methodology based on social spider optimizers (SSO) to determine the optimal sizing of an HRES-integrated microgrid. This group comprises PV, WT, battery, DG, and inverter with COE as fitness function and was presented for sensitivity analysis of sizing different topologies of MG, including PV/battery/DG, WT/battery/DG, and PV/WT/battery/DG in Aljouf Region, Saudi Arabia. Another study [11] focused on the application of the grasshopper optimization algorithm (GOA) in the area of microgrid system sizing design problems in order to determine the optimal system configuration comprising PV, WTs, BSS, and DGs with COE as a single objective

function in Yobe State, Nigeria. In [33], a novel bonobo optimizer (BO) technique was applied to find the optimal design for an off-grid HRES that contains a DG, PV, a WT, and batteries as a storage system in Saudi Arabia. It is based on annualized system cost (ASC) minimization and power system reliability enhancement. A hybrid power generation system consisting of DGs, PV systems, and battery energy storage (BES) has been optimized on the basis of BES dispatch (OBD) by considering two objectives in Indonesia: the levelized cost of energy (LCOE) and renewable energy (RE) [34].

A particle swarm optimization (MOPSO) method was proposed in [6], which dealt with the optimization problem consisting of COE and LPSP minimization for an HMS system and has been tested on three selected stations in Iran. Elsewhere, the authors of [35] proposed a multiobjective problem formulation to solve the optimization task with a self-adaptive differential evolution (DE) algorithm. This latter research has been used to analyze LPSP, COE, and RF for the city of Yanbu, Saudi Arabia for three cases of load profile. Another study presented a multiobjective evolutionary algorithm to optimally design an HMS considering load uncertainty [36]. A MOGOA was applied in [37] to optimize a microgrid with a rule-based energy management scheme. In [38], an HMS system comprising PV, wind, and battery with a diesel generator was introduced to supply load demand in Shlateen, Egypt with two planning scenarios. The first is PV/wind/battery and the second is PV/wind/battery/diesel. A multiobjective optimization problem has been solved by considering three objective functions—COE, LPSP, and RF—based on MODA. A hybrid photovoltaic, diesel, and battery nanogrid system installed in Saudi Arabia has been introduced and optimized by the parallel multiobjective PSO-based approach (PMOPSO) in [39].

Table 1 summarizes the details of the reported approaches.

Table 1. Summary of reported methods in optimizing HRES.

Reference	Year	Location	Objective Function	Algorithm
Bouchekara, H.R.E.H. [36]	2021	Saudi Arabia	Minimize the Annual LPSP/COE	Multiobjective Evolutionary Algorithm
Bukar, A.L. [37]	2020	Nigeria	Minimize the Annual COE/DPSP	Multiobjective Grasshopper Optimization Algorithm
Bouchekara, H.R. [39]	2021	Saudi Arabia	Minimize the Annual COE/LPSP	Parallel Multiobjective PSO (PMOPSO)
Farh, H.M.H. [33]	2022	Saudi Arabia	Minimize the total Annualized System Cost (ASC)	Bonobo Optimizer
Seedahmed, M.M. [22]	2022	Saudi Arabia	Minimize the Annual COE	HOMER
Thirunavukkarasu, M. [23]	2021	India	Minimize the Annual NPC/COE	HOMER
Fathy, A. [32]	2020	Saudi Arabia	Minimize the Annual COE	Social Spider Optimizer
Omar, A.S. [38]	2019	Egypt	Minimize the Annual LPSP/COE and Maximize RF	Multiobjective Dragonfly Algorithm (MODA)
Bukar, A.L. [12]	2019	Nigeria	Minimize the Annual COE	Grasshopper Optimization Algorithm
Zhu, W. [40]	2020	China	Minimize the Annual CACS/DPSP	Multiobjective Grey Wolf Optimizer

These algorithms are flexible; they avoid falling into the trap of local optima and offer a better solution than other methods. In addition, these methods have various advantages that make them worthy of solving any kind of optimization problem because they simulate the problem-solving methods used by creatures and they offer promising results in solving such problems, but the same algorithm may show poor performance in another optimization problem [11]. However, based on the free lunch theory, it is always

possible to develop new methods or algorithms that can solve the problem in a better way than the existing techniques [36]. To overcome these above-mentioned defects, MOSSA is chosen because of its simplicity, ease of use, and requirement of fewer control parameters, as it has shown impressive results in solving other engineering problems.

1.2. Article Contribution and Organization

To date, no study has been performed to show the effectiveness of MOSSA in multiobjective optimization of an HMS. MOSSA is a novel nature-inspired meta-heuristic optimization algorithm. The objective of this research paper is to design the optimal configuration of an HMS system. The main contributions of the paper can be summarized as follow:

- Determination of the optimal sizing of PV, WT, BT, DG, and inverter integrated HMS based on a recent approach called MOSSA;
- A rule-based EMS that manages the energy flow between different HRESs is proposed;
- Analysis is performed using solar radiation, wind speed, and ambient temperature data obtained from the Djelfa region in Algeria;
- The multiobjective optimization approach considered COE and LPSP as objective functions and renewable factor (RF) as a constraint.

The obtained results from MOSSA are compared with three algorithms: MODA, MOGOA, and MOALO. The comparison clearly shows that MOSSA performs better, with very fast convergence and balance between exploitation and exploration.

The rest of this paper is organized as follows: Section 2 is dedicated to the modeling of the hybrid microgrid system components, Section 3 presents the study site and the system specifications, Section 4 focusses on the proposed EMS. Whereas, Section 5 presents the obtained results based on the used optimization technique, and Section 6 contains discussion on the obtained results. This paper ends with a conclusion.

2. Modeling of Hybrid Microgrid System Components

The stand-alone microgrid of the HRES proposed in the present study is composed of two renewable energy sources (PV system, WT), an energy storage unit (battery), a backup power source (DG), and two types of loads. The PV system, WT, and battery are connected to the DC bus via bidirectional converters; in contrast, DG, load, and dump load are connected directly to the single-phase AC bus. Figure 1 shows the whole configuration of the studied stand-alone microgrid system. It is worthy to clarify that this stand-alone microgrid system is designed to be a low-voltage distribution network 220 V, 50 Hz that supplies power to a single-phase AC power system.
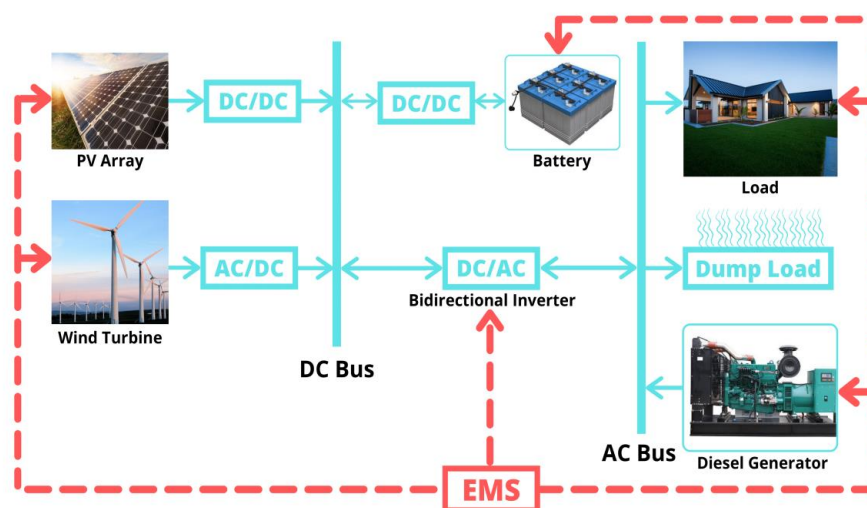

Figure 1. Stand-alone microgrid system configuration.

2.1. PV Array Modeling

The photovoltaic (PV) panels are obtained based on appropriate connections of photovoltaic cells. To provide the required output voltage in the PV panel, PV cells are connected in series to form a string. On the other side, to increase the output current capability of a panel, similar strings are connected in parallel, which forms a PV panel or a PV module whose output power rating is obtained by multiplying the voltage and the current at the output side [26,32,41].

In [42], several models were developed for the calculation of PV panel output power P_{pv_out}. However, in this study, a simple model has been used which takes into consideration two variables: ambient temperature and solar irradiance. The output power of this model can be obtained as follows [6,11,43,44]:

$$P_{pv\_out}(t) = P_{N\_pv} \times \frac{G_t(t)}{G_{t\_STC}} \times \left[1 + \alpha_t \left(T_C(t) - T_{C\_STC}\right)\right] \tag{1}$$

where P_{pv_out} is the output power of the PV module (W); P_{N_pv} is the rated power (W) of the PV module at standard test condition (STC), which is usually stipulated by the manufacturer, G_t is the solar irradiance (W/m^2); G_{t_STC} is the solar irradiance at STC ($G_{t\_STC} = 1000 \, W/m^2$); α_t is the temperature coefficient, its value is $\alpha_t = -3.7 \times 10^{-3} 1/^\circ C$ for the mono- and polycrystalline (Si) solar cells [45,46]; T_{C_STC} is the cell temperature at STC ($T_{C\_STC} = 25\,^\circ$); and T_{amb} is the ambient temperature ($^\circ$C).

The cell temperature T_c is calculated by the following expression [44]:

$$T_C(t) = T_{amb}(t) + [0.0256 \times G_t(t)] \tag{2}$$

2.2. Wind Turbine Modeling

The output power of the wind turbine generator varies following variation of wind speed, which is a function of the height at the same location. Thus, the measured wind speed at the anemometer height must be adjusted to the used hub height of the wind turbine [12]. In this context, two mathematical models are used for the determination of the wind speed vertical profile of a specific location such as the log-law and the power-law [47,48].

In this study, the determination of the wind profile is obtained by using the power-law model as follows [48]:

$$\frac{V_2}{V_1} = \left(\frac{h_2}{h_1}\right)^\alpha \tag{3}$$

where $V_2 (m/s)$ is the wind speed at the hub height $h_2 (m)$, $V_1 (m/s)$ is the wind speed at the reference height $h_1 (m)$, and α is the friction coefficient (also known as: Hellmann exponent, wind gradient, or power-law exponent). α is a function of varying parameters such as wind speed, roughness of terrain, height above ground, temperature, hour of the day, and time of the year [6,49–51]. The value of the friction coefficient can be considered to be 0.11 at extreme wind conditions and 0.2 at normal wind conditions as specified by Standard IEC 61400-1 [49,52,53]. However, a value of ($\alpha = 1/7$) is commonly accepted [6].

The output power of wind turbine generator can be evaluated based on the following equation [54–56]:

$$P_{wt}(t) = \begin{cases} 0 & V < V_{cut-in} \\ V^3 \left(\frac{P_r}{V_r^3 - V_{cut-in}^3}\right) - P_r \left(\frac{V_{cut-in}^3}{V_r^3 - V_{cut-in}^3}\right) & V_{cut-in} \leq V < V_{rated} \\ P_r & V_{rated} \leq V \leq V_{cut-out} \\ 0 & V > V_{cut-out} \end{cases} \tag{4}$$

where P_r is the rated power (kW); V is the wind speed (m/s); V_{cut_in}, V_{rated}, $V_{cut-out}$ represent the cut-in, rated, and cut-out wind speed of the WT, respectively in m/s. These

values are usually stipulated by the manufacturer. Figure 2 shows the output power of the wind turbine generator versus the wind speed at the height of the hub.
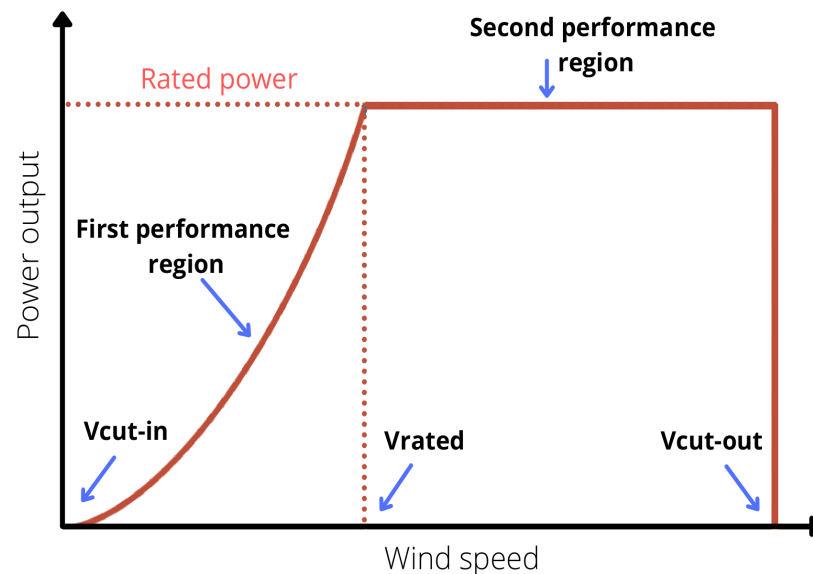

Figure 2. Variation of wind turbine generator power with wind speed.

The rated power P_r (W) of a wind turbine generator is expressed as a function of the area swept by the blades A_{wind}, the maximum power coefficient C_p, the air density ρ_{air}, and the rated wind speed, as follows [55]:

$$P_r = \frac{1}{2}C_p \times \rho_{air} \times A_{wind} \times V_r^3 \tag{5}$$

2.3. Battery Bank Modeling

The battery system is an important unit in the stand-alone microgrid and ensures supply of the load when the power generated from renewable energy sources is insufficient.

Battery capacity can be calculated as follows [57,58]:

$$C_{Batt} = \frac{AD \times P_{load}}{\eta_{Inv} \times \eta_{Batt} \times DOD} \tag{6}$$

where P_{load} is the power demand of the load, η_{Inv} is the inverter efficiency, η_{Batt} is the battery efficiency, DOD is the battery depth of discharge, and AD is the days of autonomy, which is defined as the number of days that the battery will be able to supply the required power demand of the load without deficiency.

It is obvious that the energy generated from renewable energy sources (PV and WT) depends on wind speed and solar radiation, which are intermittent in nature; therefore, days of autonomy is of great importance and must be taken into account while sizing the battery bank to overcome the problem of power deficit production from these sources. In case of energy production excess, the excess is used to charge the battery. The power produced from the battery bank can be expressed as follows [40]:

$$P_{Batt}(t) = \left(P_{pv}(t) + P_{wt}(t)\right) - \frac{P_{load}(t)}{\eta_{Inv}} \tag{7}$$

where $P_{pv}(t)$, $P_{wt}(t)$, and $P_{load}(t)$ represent the power produced from PV, WT, and load power demand, respectively, and η_{Inv} is the inverter efficiency.

When $P_{Batt}(t) < 0$, this indicates that there is an energy generation deficit. Otherwise, if $P_{Batt}(t) > 0$, it indicates that the energy generation exceeds the power demand. In the

rare case that $P_{Batt}(t) = 0$, the generated power from the renewable sources is equal to the load power demand.

For checking the state of the battery bank, the state of charge (SOC) of the battery is an important parameter that affects battery performance and indicates its current capacity. Indeed, the SOC can be defined following both the states of charging and discharging as follows [59,60]:

- Charging process, if; $P_{pv}(t) + P_{wt}(t) > P_{load}(t)$

$$SOC(t) = SOC(t-1) \times (1 - \sigma) + \left((P_{pv}(t) + P_{wt}(t)) - \frac{P_{load}(t)}{\eta_{Inv}} \right) \times \eta_{Batt} \quad (8)$$

- Discharging process, if; $P_{pv}(t) + P_{wt}(t) < P_{load}(t)$

$$SOC(t) = SOC(t-1) \times (1 - \sigma) + \left(\frac{P_{load}(t)}{\eta_{Inv}} - (P_{pv}(t) + P_{wt}(t)) \right) \times \eta_{Batt} \quad (9)$$

2.4. Diesel Generator Modeling

The diesel generator is used as a backup source if the renewable energy sources and battery bank are insufficient to meet the load power demand requirement. The following equation can be used to calculate the hourly fuel consumption of the diesel generator [61,62]:

$$F_{DG}(t) = \alpha P_{DG}(t) + \beta P_r \quad (10)$$

where $F_{DG}(t)$ is the generator fuel consumption (L/hr), $P_{DG}(t)$ is the generated power (kW), P_r is the capacity of the generator (kW), α is the fuel curve slope coefficient $(L/hr/kW_{output})$, and β is the fuel intercept coefficient $(L/hr/kW_{rated})$. α and β used in the present study are taken as $\alpha = 0.246$ and $\beta = 0.08415$ [61,62].

The efficiency of the diesel generator can be calculated as [63]:

$$\eta_{overall} = \eta_{brake-thermal} \times \eta_{generator} \quad (11)$$

where $\eta_{overall}$, $\eta_{generator}$, and $\eta_{brake-thermal}$ represent the overall efficiency, generator efficiency, and brake thermal efficiency of the diesel generator, respectively.

2.5. Inverter Modelling

The inverter converts the electrical energy from direct current (DC) to alternating current (AC). The inverter's efficiency is defined as follows [6,64,65]:

$$\eta_{inv} = \frac{P}{P + P_0 + KP^2} \quad (12)$$

where P, P_0, and K can be calculated by the following equations [6,64,65]:

$P = P_{out}/P_n$

$P_0 = 1 - 99(1/\eta_{10} - 1/\eta_{100} - 9)^2$

$K = 1/\eta_{100} - P_0 - 1$

where P_n is the inverter's rated power and η_{10} and η_{100} are the efficiencies of the inverter at 10 and 100% of the rated power, respectively. Both η_{10} and η_{100} are stipulated by the manufacturer.

3. Definition of the Study Site and System Specifications

3.1. Location and Meteorological Conditions

The proposed stand-alone microgrid of the hybrid renewable energy system is supposed to be located in Aïn El Ibel, Djelfa in the north-central region of Algeria at 34.346° latitude and 3.163° longitude. It is situated in a transitional zone between the dry high plains in the north and the desert in the south. The area is characterized by very hot

weather in the summer and very cold weather in winter, with high wind speeds in the winter. Figure 3 shows the geographical location of the study site, while Table 2 presents the related background information and the period of data measurement.
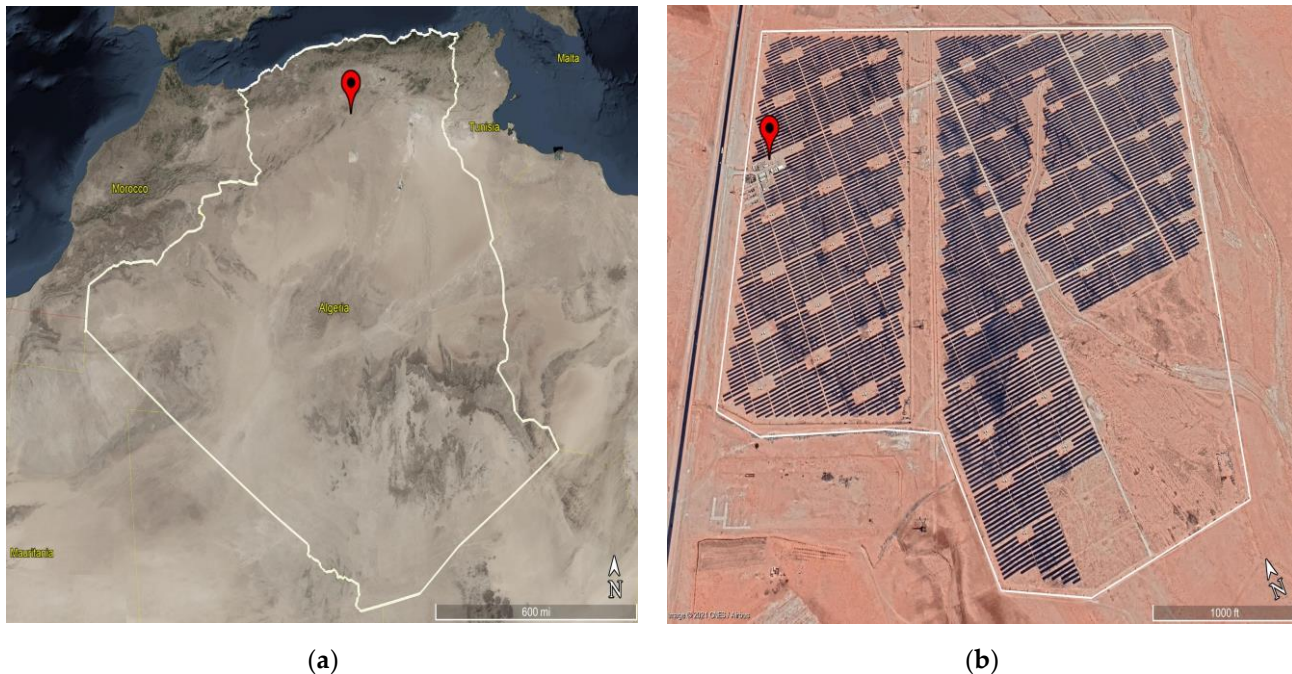

(**a**)　　　　　　　　　　　　　　　　　　　　　　　　　(**b**)

Figure 3. The geographical map of the study location using Google Earth. (**a**) Map of the selected location; (**b**) close look at the selected location.

Table 2. Geographical coordinates of the study site.

Particulars	Details
Country	Algeria
State	Djelfa
District	Aïn El Ibel
Municipality	Aïn El Ibel
Latitude	34.346°
Longitude	3.163°
Altitude above sea level	1098 m
Study site	Central PV Aïn El Ibel (SKTM)
Period of measurement	1 January 2020–31 December 2020

Wind speed, solar radiation, and ambient temperature used for the simulations in this study were obtained from the National Aeronautics and Space Administration (NASA) [66] at the coordinates of Aïn El Ibel (34.346° latitude and 3.163° longitude). The average solar radiation of the selected location during the mentioned year is 0.2357 KW/m^2, the average wind speed is 4.3467 m/s, and the average ambient temperature is 290.4010 K. Figures 4–6 show the hourly solar radiation profile, the wind speed at the height of 10 m above ground level, and the ambient temperature over a year (8784 h).
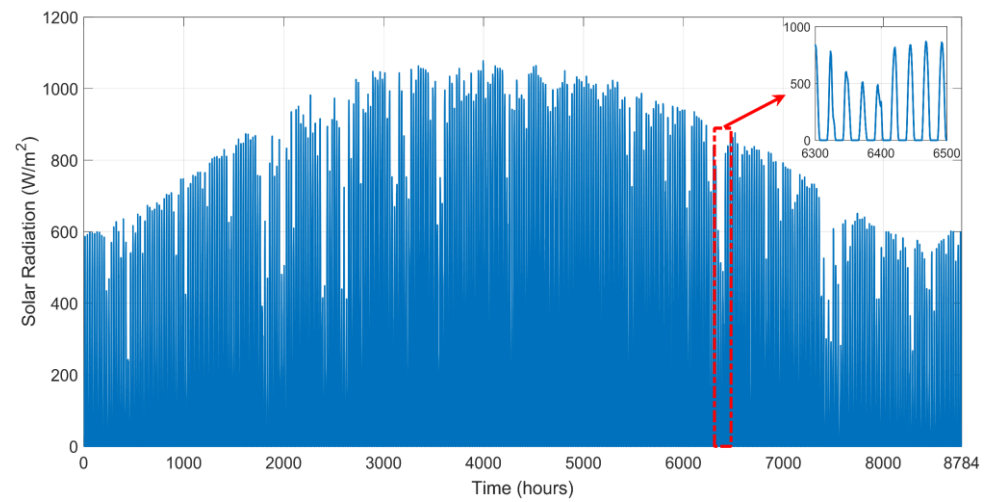
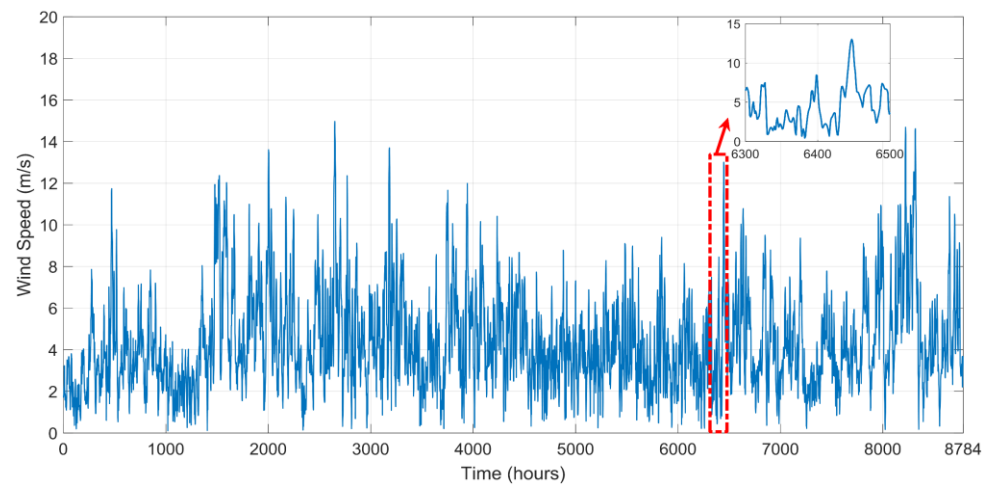**Figure 4.** Annual solar radiation of the studied site.

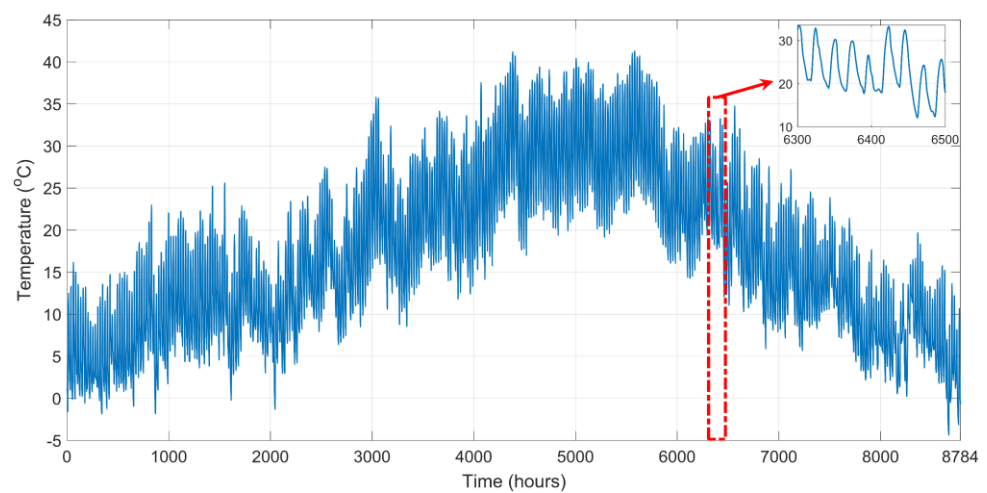**Figure 5.** Annual wind speed of the studied site.

Figure 6. The annual ambient temperature of the studied site.

3.2. Load Assessment

To design a reliable and efficient stand-alone microgrid based on renewable energy sources system for a specific location, the load profile must be defined precisely. Indeed, it

is obvious that the fluctuating nature of the load affects the system reliability, the number of components, and the price of the produced electrical energy. Therefore, in the present study, it is supposed that the studied stand-alone microgrid will power a specific load of a residential area composed of a group of homes with each home presented as a residential unit as detailed in Table 3.

Table 3. Power-consuming appliances needed for the residential units.

Appliances	Power (W)	Quantity	Electric Load (W)
Refrigerator	220	2	440
Television	150	3	450
Mobile Charger	12	6	72
Water Pump	450	2	900
Radio	12	1	12
Lamps Bulb	75	5	375
Lamps CFL	18	8	144
Fluorescent Light	40	5	200
Laptop	46	3	138
Desktop computer	120	2	240
Mixer	450	1	450
Deep freezer	260	1	260
Air conditioner	430	2	860
Washing machine	420	1	420
Microwave	900	1	900

The microgrid is analyzed for ten residential units in an off-grid community. The studied load profile is presented within the four seasons of the year—winter, spring, summer, and autumn—and has an average annual power consumption of 12.04545 kW. Figures 7 and 8 present the hourly load profile of the residential units.
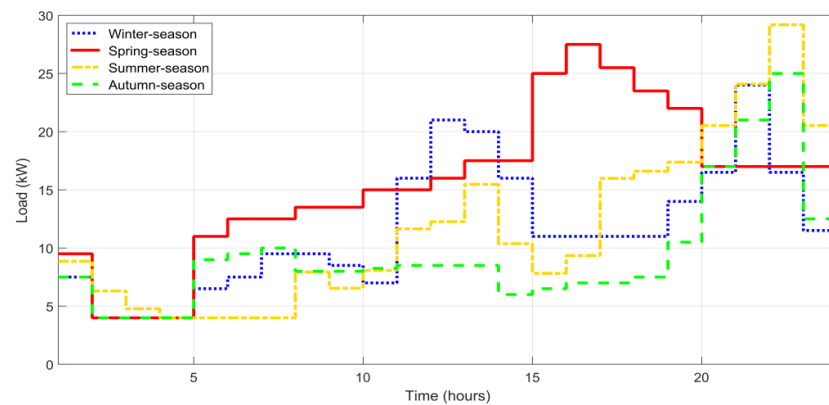

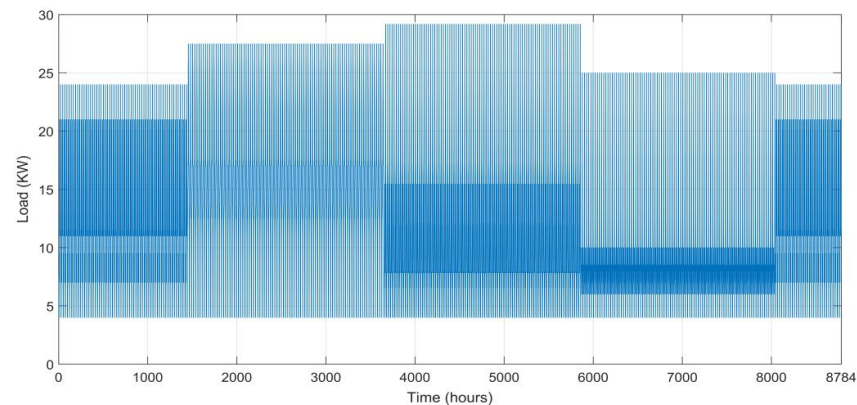**Figure 7.** Load profile in the winter, spring, summer, and autumn seasons.

Figure 8. Hourly load profile for the residential units.

3.3. Specifications of Hybrid Microgrid System Components

The economic and technical parameters of hybrid microgrid system components used in this study are listed in Table 4:

Table 4. Technical and economic specifications of the HMGS components [6,32,36].

Component	Parameter	Value	Unit
Photovoltaic	Rated power	7.3	kW
	PV regulator efficiency	95	%
	Lifetime	24	Year
	PV regulator cost	1500	$
	Initial cost	2150	$/kW
Wind Turbine	Model	Eolica 2 kW	
	Rated power	2	kW
	Cut-in wind speed	2.0	m/s
	Rated wind speed	9.0	m/s
	Cut-out wind speed	20.0	m/s
	Number of blades	3	m
	Tower height	20	%
	Efficiency	95	Year
	Lifetime	24	$
	Wind turbine regulator cost	1000	$/kW
	Price	2000	
Battery	Rated power	40	kW h
	Efficiency	85	%
	Lifetime	2	Year
	SOC_Min	30	%
	SOC_Max	100	%
	DOD	70	%
	Initial cost	220	USD/kW h
Diesel Generator	Rated power	4	kW
	Lifetime	24,000	hours
	Initial cost	1000	USD/kW h
Inverter	Lifetime		Year
	Efficiency	24922500	%
	Initial cost		$
Economic Parameters	Project lifetime	24	Year
	Fuel inflation rate	5	%
	O&M + Running cost	20	%
	Real interest	13	%
	Discount rate	8	%

4. Energy Management Strategy of Hybrid Microgrid System

The energy management strategy (EMS) is one of the main criteria to be considered when designing or sizing an autonomous microgrid which is intended to ensure the distribution and management of power flow among the various elements of the studied stand-alone microgrid system. The main targets of the proposed EMS can be summarized as follows:

- System efficiency enhancement, thus achieving low cost and energy-saving benefits;
- Maximization of utilization of the renewable energy sources (PV and WT);
- Protection of the battery bank and minimization of its degradation;
- Minimization of fuel consumption.

In this study, four modes of energy management strategy (EMS) have been used:

- Mode 1: In this mode, the generated power from renewable energy sources (PV and WT) is sufficient to supply the load demand requirement. The extra energy is used to charge the battery bank system;

- Mode 2: In this mode, the generated power from the renewable energy sources exceeds the load demand requirement while the battery is fully charged. In this case, the surplus of energy is consumed in a dump load;
- Mode 3: In this mode, the generated power from the renewable energy sources is less than the load demand requirements. In this case the battery bank will cover the power generation deficiency to fit the load demand requirements;
- Mode 4: In this mode, the power generated from the renewable energy sources is not sufficient to meet the load demand requirement and at the same time, the battery bank storage level is low. In this case, the diesel generator will operate to cover the gap in power generation to fit the load demand requirement and further ensure the battery bank's charging

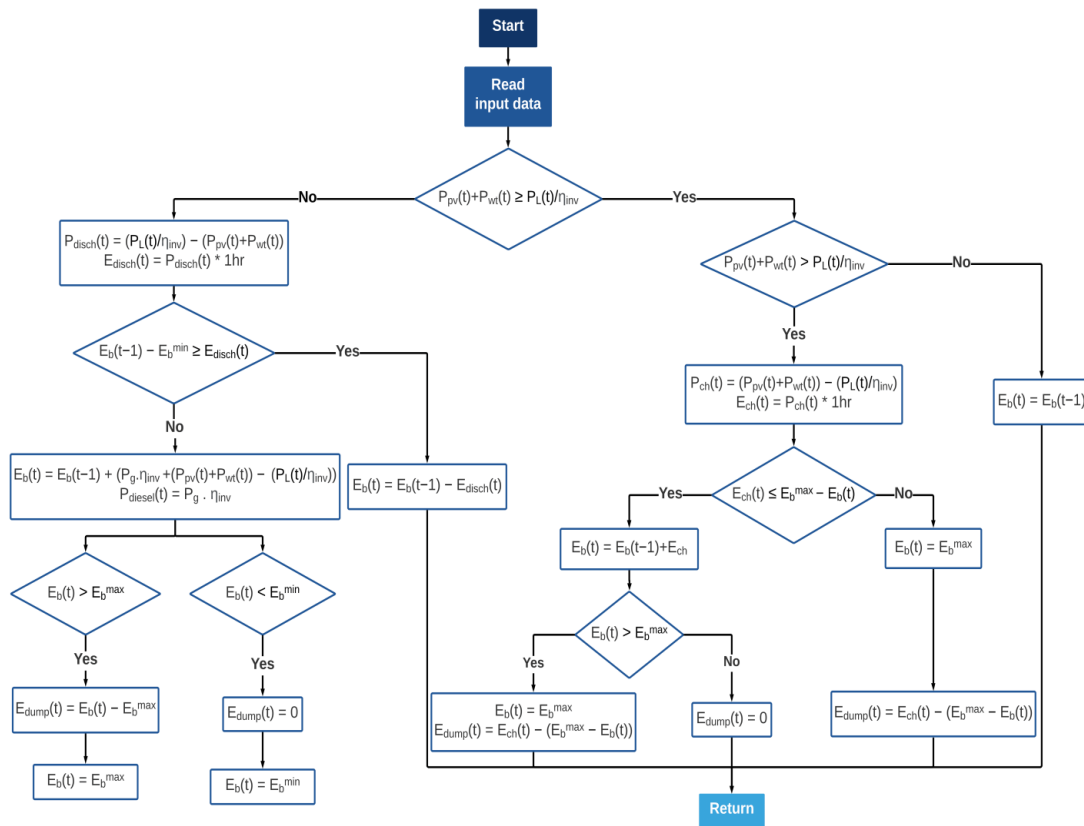Figure 9 shows the flowchart of the proposed EMS algorithm used in the presen study.

Figure 9. The proposed rule-based energy management strategy.

5. Optimization Problem Formulation of the Studied Stand-Alone Microgrid

5.1. Multiobjective Optimization

In this work, the optimization problem of the studied hybrid microgrid system (HMGS) is based on solving a multiobjective optimization problem which is formulated as follows:

$$
\text{Minimize} : f(x) = \begin{bmatrix} f_1(x) \\ f_2(x) \\ \cdot \\ \cdot \\ \cdot \\ f_n(x) \end{bmatrix} \tag{13}
$$

$$
\text{Subjected to} \begin{cases} H(x) = 0 \\ G(x) \leq 0 \end{cases} \tag{14}
$$

where $f(x) = [f_1(x), f_2(x), \ldots \ldots, f_n(x)]$ is the vector of the objective functions and n is the number of objective functions, $f_i(x)$ is the objective function number i, $x = [x_1, x_2, x_3, \ldots \ldots \ldots \ldots, x_n]$ is the vector of the variables to be designed, $H(x)$ is the set of equality constraints, and $G(x)$ is the set of inequality constraints.

5.2. Objective Functions

In order to evaluate microgrid performances, the loss of power supply probability (LPSP) and the cost of energy (COE) are proposed as objective functions, where the main aim is to minimize these two functions in order to maintain the high reliability and the lowest cost of the studied HMGS.

5.2.1. Loss of Power Supply Probability

The reliability of the microgrid system is evaluated based on LPSP . It is a statistical term which indicates the probability of power supply failing to meet the load demand requirement due to technical problems or because the energy produced from renewable sources is insufficient to meet the load demand requirement. The LPSP can be calculated using the following equation [67,68]:

$$\text{LPSP} = \frac{\sum \left(P_{load} - P_{pv} - P_{wt} + P_{SOC\_min} + P_{diesel} \right)}{\sum P_{load}} \tag{15}$$

where the value of LPSP is in the range between [0, 1]. If its value is equal to zero, the load energy demand is fully satisfied. On other hand, if the LPSP equal to unity, the load energy demand is not satisfied.

In this work, the evaluation of the system's reliability is taken within the worst conditions as follows [6,35]:

$$P(t)_{load} > P(t)_{generate} \tag{16}$$

where $P(t)_{generate}$ denotes the power generated. It should be noted that under this condition, the total load energy demand is greater than the entire energy generation from all the available sources.

5.2.2. Cost of Energy

The COE is one of the most important indicators of the economic profitability of HRES integrated in microgrid [6,69]. It is defined as the unit of cost per unit of energy production from the HRES (USD/kW h), and it can be calculated for each component of the studied microgrid based on the following equations [32,70]:

$$C_t^{PV} = N^{PV} \left(C_C^{PV} + C_{O\&M}^{PV} \times \left(\frac{(1+i)^n - 1}{i(1+i)^n} \right) \right) \tag{17}$$

$$C_t^{WT} = N^{WT} \left(C_C^{WT} + C_{O\&M}^{WT} \times \left(\frac{(1+i)^n - 1}{i(1+i)^n} \right) \right) \tag{18}$$

$$C_t^{Batt} = C_C^{Batt} + C_{O\&M}^{Batt} \times \left(\frac{(1+i)^n - 1}{i(1+i)^n} \right) + C_R^{Batt} \times \sum_{j=1}^{\left(\frac{n}{n_{Batt}} - 1 \right)} \left(1 + \frac{1}{(1+i)^{jn_{Batt}}} \right) \tag{19}$$

$$C_t^{DG} = C_C^{DG} + C_{O\&M}^{DG} \times \left(\frac{(1+i)^n - 1}{i(1+i)^n} \right) + C_R^{DG} \times \sum_{j=1}^{\left(\frac{n}{n_{Batt}} - 1 \right)} \left(1 + \frac{1}{(1+i)^{jn_{DG}}} \right) \tag{20}$$

The resulting net cost of the four sources can be calculated as follows:

$$\text{NPC} = C_t^{PV} + C_t^{WT} + C_t^{Batt} + C_t^{DG} + C_t^{Inv} \tag{21}$$

where C_t^{PV}, C_t^{WT}, C_t^{Batt}, C_t^{DG}, and C_t^{Inv} are the energy costs of PV system, WT system, battery bank, and diesel generator, respectively; C_C^{PV}, C_C^{WT}, C_C^{Batt}, and C_C^{DG} represent

the investment costs put into these sources of energy, respectively; $C_{O\&M}^{PV}$, $C_{O\&M}^{WT}$, $C_{O\&M}^{Batt}$, and $C_{O\&M}^{DG}$ are the operation and maintenance costs of PV, WT, battery bank, and diesel generator, respectively; C_R^{Batt} and C_R^{DG} are the replacement costs of the battery bank and the diesel generator, respectively; i is the annual interest; n is the system life time; and n_{Batt} and n_{DG} are the life time of the battery bank and the diesel generator, respectively. The COE can be calculated as follows [69]:

$$COE = \frac{NPC}{\sum_{h=1}^{8784} P_{load}} \times CRF \tag{22}$$

where P_{load} is the hourly power consumption and CRF is the capital recovery factor, which is defined as follows [71]:

$$CRF = \frac{i(1+i)^n}{(1+i)^n - 1} \tag{23}$$

5.3. Constraints

Renewable Factor

The renewable factor (RF) is a factor that determines the amount of power generated from renewable resources in comparison to non-renewable resources (diesel generator) used in the microgrid, and it is expressed as follows [36]:

$$RF(\%) = \left(1 - \frac{\sum P_{diesel}}{\sum P_{pv} + \sum P_{wt}}\right) \times 100 \tag{24}$$

when the RF equals 100%, it means that the system is in an ideal state and is dependent only on power generated from renewable energy resources. When it equals zero percent, it means that the power coming from the diesel generator is equivalent to the power generated from renewable energy resources.

5.4. Design Variables

The design variables considered in this study are the nominal power of the photovoltaic system (PV), the number of wind turbines (N^{WT}), and the number of autonomy days (N^{AD}). The constraints on the proposed design variables are given as follows:

$$\text{Design variables}: \begin{cases} 0 \leq PV \leq 80 \\ 0 \leq N^{WT} \leq 10 \\ 0 \leq N^{AD} \leq 3 \end{cases} \tag{25}$$

5.5. Multiobjective Salp Swarm Algorithm

Salp swarm algorithm (SSA) is a new swarm intelligence algorithm that belongs to the family of metaheuristic optimization algorithms. It has been proposed based on the foraging behaviors of salps and their intelligence, which was proposed by Mirjalili et al. in 2017 [72]. After the food source is detected in salp lookup mechanisms, salps gather in chains to search for food sources using these chains. Each series will follow the lead salp (the leader), and the leader will direct and lead the other salps to catch the food source [73]. The shape of a salp is shown in Figure 10a, and the salp chain is illustrated in Figure 10b.
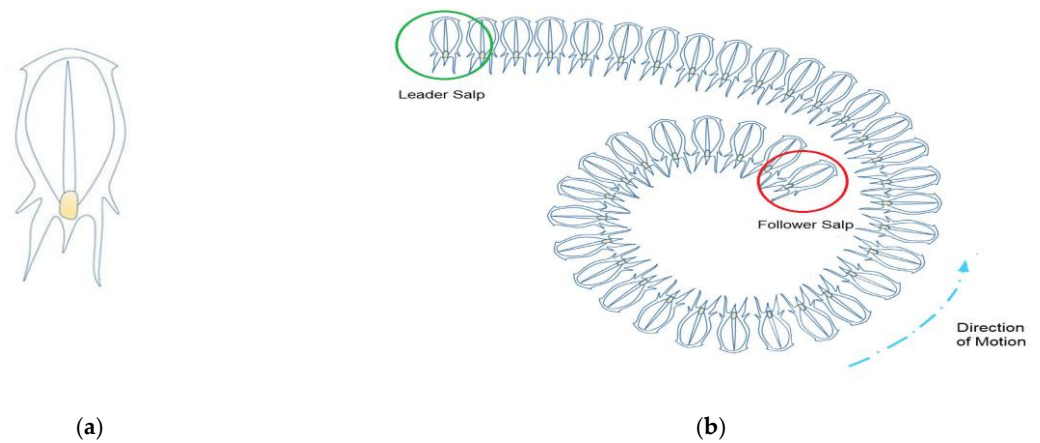
(a)   (b)

Figure 10. Swarm of salps. (**a**) Individual salp; (**b**) salp chain [74].

5.5.1. Basic Salp Swarm Algorithm

The salp leader moves toward the food source named (F_j) in the search space, while all followers can move toward the rest of the salp. The position of the salps is specified in the n-dimensional search space, where n is the number of variables for a given problem. Therefore, the position of all the salps is stored in a two-dimensional matrix called X_i with a size of $N \times d$, as described in the flowing equation [75]:

$$X_i = \begin{bmatrix} x_1^1 & x_2^1 & \cdots & x_d^1 \\ x_1^2 & x_2^2 & \cdots & x_d^2 \\ \vdots & \vdots & \cdots & \vdots \\ x_1^N & x_2^N & \cdots & x_d^N \end{bmatrix} \tag{26}$$

The update of the leader's position is performed based on the following equation [72]:

$$x_j^1 = \begin{cases} F_j + c_1\big((ub_j - lb_j)c_2 + lb_j\big) & c_3 \geq 0 \\ F_j - c_1\big((ub_j - lb_j)c_2 + lb_j\big) & c_3 < 0 \end{cases} \tag{27}$$

where x_j^1 is the position vector of the first salp (the leader) in the jth dimension, F_j is the position vector of the food source in the jth dimension. ub_j and lb_j represent the upper bound and the lower bound of the jth dimension, respectively. c_1, c_2, and c_3 are random numbers that uniformly generated with values between [0, 1]. As indicated in Equation (7), the leader will only update its position with respect to the food source.

The coefficient c_1 balances between the exploration and exploitation, so it is considered one of the most important parameters in salp swarm algorithms (SSA), and it is defined as follows [72]:

$$c_1 = 2e^{-\left(\frac{4l}{L}\right)^2} \tag{28}$$

where l indicates the current iteration, and L indicates to the maximum number of iterations.

The followers update their positions based on Newton's law of motion as follows [72]:

$$x_j^i = \frac{1}{2}at^2 + v_0t \tag{29}$$

where $i \geq 2$, x_j^i is the position vector of the ith follower salp in the jth dimension, t is the time, v_0 is the initial speed, and $a = \frac{v_{final}}{v_0}$ where $v = \frac{x - x_0}{t}$.

Because the time in optimization represents the iteration based on a specified sampling unit, the discrepancy between iterations is equal to 1, and by considering that $v_0 = 0$, the aforementioned equation can be expressed as follows [72]:

$$x_j^i = \frac{1}{2}\left(x_j^i + x_j^{i-1}\right) \tag{30}$$

where $i \geq 2$, and x_j^i is the follower salps' position vector in the jth dimension. According to the mathematical simulation described in the above equations, the swarm behavior of the salp chains can be clearly understood and easily simulated.

5.5.2. Multiobjective Salp Swarm Algorithm

A set of solutions called the Pareto group presents the solution to the problem of multiple objective function optimization. The SSA algorithm is based on the movement of the salps towards the food source and updating their position over the course of iterations. This first problem is addressed by equipping the SSA algorithm with a food source repository. This repository holds the best nondominant solutions obtained so far during optimization. The multiobjective salp swarm algorithm (MOSSA) approach inherits the SSA operators due to the similar population division (leader and follower salps) and the position updating process. The MOSSA algorithm is logically capable of finding the perfect Pareto solutions with high distribution across all objective functions [75–77]. The MOSSA pseudo-code is represented in Algorithm 1.

Algorithm 1. Pseudo code of the MOSSA algorithm [72,78]

---

1   Set the hyper-parameter:
2   Max_iter: Maximum of iteration
3   ArchiveMaxSize: Max capacity of archive (repository)
4   Dim: The number of parameters on each salp
5   ub_j and lb_j: The upper bound and the lower bound of salp population
6   Obj-no: The objective number to be estimated
7   Initialize the salp population $x_i (i = 1, 2, \ldots, n)$ considering ub_j and lb_j
8   Define the objective function (loss function): @ Ob-func
9   **while** *(end criterion is not met)* **do**
10   Calculate the fitness of each search agent (salp) with Ob-func
11   Determine the non-dominated salps
12   Update the repository considering the obtained non-dominated salps
13   **if** *(the repository becomes full)* **then**
14   Call the repository maintenance procedure to remove one repository resident
15   Add the non-dominated salp to the repository
16   **end**
17   Choose a source of food from repository: F = SelectFood (repository)
18   Update c_1 by $c_1 = 2e^{-\left(\frac{4l}{L}\right)^2}$
19   **for** *each salp x_i:* **do**
20   **if**$(i == 1)$**then**
21   Update the position of the leading salp by:
22          $x_j^1 = \begin{cases} F_j + c_1\left(\left(ub_j - lb_j\right)c_2 + lb_j\right) & c_3 \geq 0 \\ F_j - c_1\left(\left(ub_j - lb_j\right)c_2 + lb_j\right) & c_3 < 0 \end{cases}$
23   **else**
24   Update the position of the follower salp by:
25          $x_j^i = \frac{1}{2}\left(x_j^i + x_j^{i-1}\right)$
26   **end**
27   **end**
28   Amend the salps based on the upper and lower bounds of variables
29   **end**
30   **return** repository

To solve the sizing problem, MOSSA is used to follow several procedures. The proposed procedure of actions is defined in detail in Figure 11. When the simulation begins, like any other optimization algorithm, MOSSA places random particles in the search landscape, whose bounds are set by the user. According to the algorithm's governing equations, these particles move around the search landscape, optimizing the defined objective function. To validate the effectiveness and performance of the MOSSA, the developers have carried out a series of tests, in which the performance of the MOSSA is compared with other well-known optimization algorithms like the multiobjective particle swarm optimization (MOPSO) and the non-dominated sorting genetic algorithm (NSGA-II) [72], and they concluded that MOSSA balances between exploration and exploitation in a satisfactory and improved manner compared to its counterparts.
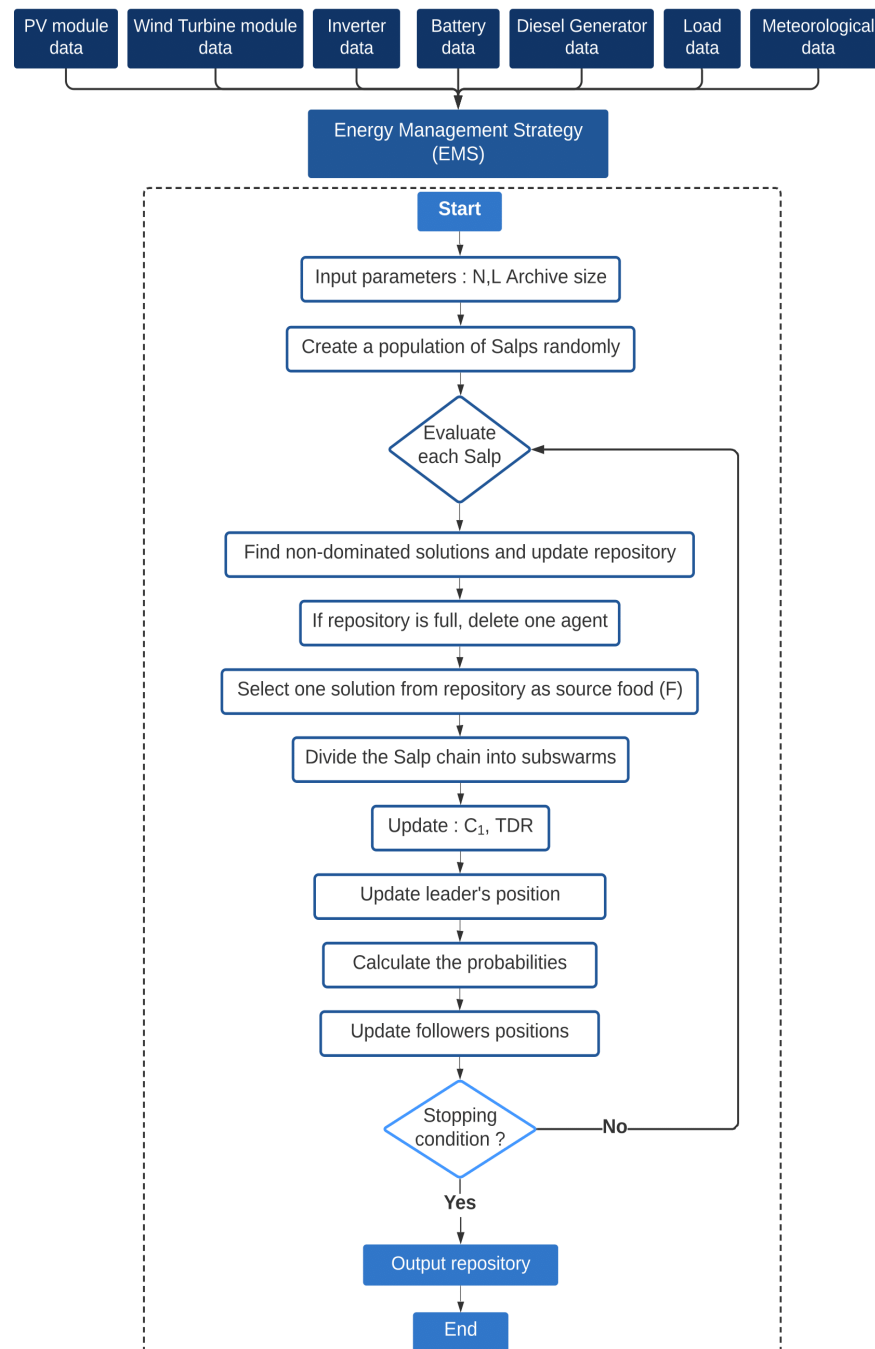

Figure 11. Flowchart of the proposed approach.

MOSSA has recently been used to solve engineering problems, such as short-term load forecasting presented by J. Wang et al. [78] and for the enhancement of electrical distribution system performances including DG and DSTATCOM simultaneously proposed by A. Lasmari et al. [75]. The authors of [75–78] have affirmed that the result of the MOSSA outperforms other approaches, namely the multiobjective grasshopper optimization algorithm (MOGOA) and the multiobjective ant lion optimizer (MOALO). These studies have verified the effectiveness of the MOSSA in solving complex optimizations problems better than the other techniques.

6. Results and Discussion

In this paper, the optimization design of a stand-alone microgrid based on hybrid renewable energy system consisting of PV/WT/battery bank with a diesel generator system as a backup source is presented. These sources' main role is to fulfill the load energy demand, which is composed of 15 residential housing units. The whole studied system has been implemented in the MATLAB R2018a environment. All tests were performed on an Intel Core i7-10510U CPU 2.30 GHz 16 GB RAM, Windows 10 Pro Version 21H2 (64-bit) personal computer.

This study comprises the application of four optimization algorithms to solve the main problem of optimization design presented in this paper:

- First Algorithm: MOSSA optimization algorithm;
- Second Algorithm: multiobjective dragonfly algorithm (MODA) [79];
- Third Algorithm: multiobjective grasshopper optimization algorithm (MOGOA) [80];
- Fourth Algorithm: multiobjective ant lion optimizer (MOALO) [81].

In a previous study [6,35], the optimization problem of HMS was treated only as a single-target optimization problem where different objective functions have been grouped into one objective function as single-objective optimization problem. This approach has the disadvantage of determining only one optimal solution. In this paper, multiple choices are offered for the optimal design of the studied microgrid based on the approach of multiobjective optimization. This approach creates a set of optimal solutions known as the Pareto front.

MOSSA, MODA, MOGOA, and MOALO have been executed along 100 iterations. Table 5 shows the different control parameters, which have been used for each proposed approach.

The solutions obtained by applying the previously mentioned methods for stand-alone microgrid configurations present an impressive and consistent distribution. Figure 12a–d presents the Pareto front of the stand-alone microgrid system obtained for each algorithm based on LPSP and COE functions.

On the Pareto front, the results show not only an optimal solution, but a group of optimal solutions (non-dominated solutions), a variety of design decision possibilities. The next section presents the obtained results of MOSSA, MODA, MOGOA, and MOALO algorithms.
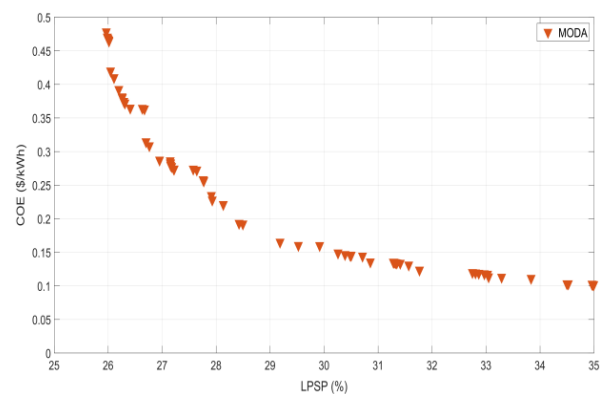
Table 6 shows 20 selected solutions from the Pareto fronts for the first algorithm as shown in Figure 12a. For more clarification, these solutions have been organized based on the COE. If solution #1 is selected by the designer, the power generated by the PV panels is 65.883 kW, the autonomy days is equal to three days, and the required number of wind turbines is ten, which ensures a power generation of 20 kW. This solution corresponds to a COE of 0.255 USD/kW h, an LPSP of 27.079%, and an RF of 90.46%. It can be noted that the COE and the RE have higher values and the LPSP has a lower value than the other available solutions.

Table 5. Parameters for each approach.

| Algorithms	Parameters
MOSSA	Population size: 100 Number of iterations: 100 Archive size: 200 The coefficient c_1: Equation (28) The coefficient c_2: rand The coefficient c_3: rand, $c_3 < 0.5$
MODA	Population size: 100 Number of iterations: 100 Archive size: 200 $w = 0.9 - 0.2$, $s = 0.1$ $a = 0.1$, $c = 0.7$ $f = 1$, $e = 1$
MOGOA	Population size: 100 Number of iterations: 100 Archive size: 200 The coefficient c_{Max}: 1 The coefficient c_{Min}: 0.00004
MOALO	Population size: 100 Number of iterations: 100 Archive size: 200 $c^t = \frac{c^t}{T}$, $d^t = \frac{d^t}{T}$
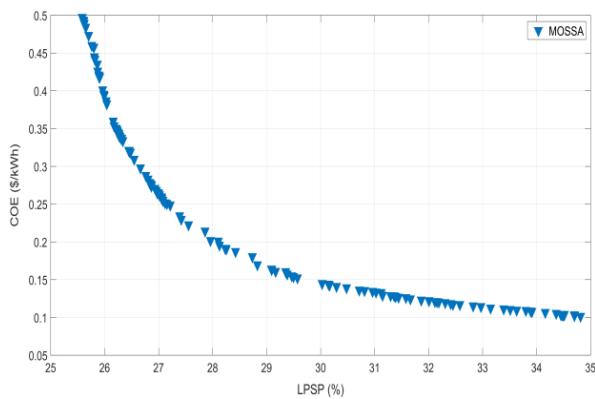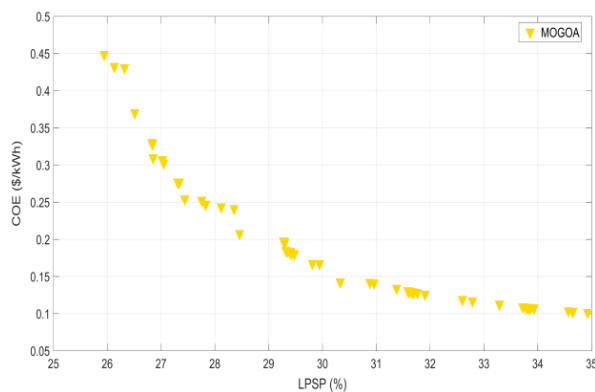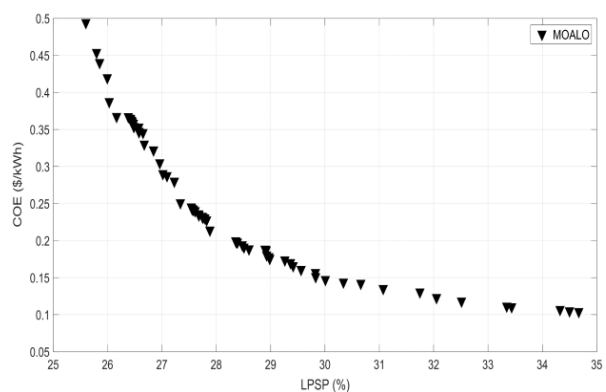
Figure 12. Pareto front of stand-alone microgrid system considering LPSP and COE. (**a**) MOSSA; (**b**) MODA; (**c**) MOGOA; (**d**) MOALO.

Table 6. Selected solutions from the Pareto front of MOSSA.

Solution #	PV (KW)	N^{AD}	N^{WT}	COE (USD/kW h)	LPSP (%)	RE (%)	The AEC from PV (MW)	The AEC from WT (MW)	The AEC from BT (MW)	The AEC from DG (MW)
Solution # 1	65.883	3	10	0.255	27.079	90.46	121.8	38.87	118.33	15.33
Solution # 2	64.715	3	10	0.252	27.118	90.31	119.64	38.87	118.18	15.36
Solution # 3	64.436	3	10	0.251	27.153	90.27	119.12	38.87	118.09	15.36
Solution # 4	63.734	2.953	10	0.249	27.213	90.17	117.82	38.87	116.21	15.4
Solution # 5	63.773	2.979	10	0.249	27.215	90.17	117.9	38.87	117.18	15.4
Solution # 6	51.454	2.721	10	0.214	27.859	88.18	95.12	38.87	105.3	15.84
Solution # 7	46.642	2.781	10	0.201	28.105	87.2	86.23	38.87	106.61	16.01
Solution # 8	44.638	3	10	0.196	28.126	86.8	82.52	38.87	114.34	16.02
Solution # 9	42.836	3	10	0.191	28.252	86.36	79.19	38.87	113.74	16.11
Solution # 10	41.726	2.711	10	0.187	28.424	85.9	77.14	38.87	102.74	16.36
Solution # 11	32.414	2.697	10	0.161	29.353	82.49	59.92	38.87	98.07	17.22
Solution # 12	30.978	2.844	10	0.158	29.382	82.04	57.27	38.87	102.35	17.27
Solution # 13	29.081	3	10	0.152	29.57	81.12	53.76	38.87	106.38	17.49
Solution # 14	26.493	2.766	10	0.145	30.028	79.41	48.98	38.87	96.35	18.09
Solution # 15	25.132	2.733	10	0.141	30.294	78.46	46.46	38.87	94.21	18.38
Solution # 16	24.935	2.711	10	0.139	30.48	77.94	46.1	38.87	92.95	18.55
Solution # 17	23.83	2.887	10	0.136	30.715	77.17	44.05	38.87	97.6	18.7
Solution # 18	23.59	2.697	10	0.135	30.962	76.61	43.61	38.87	90.98	18.9
Solution # 19	23.843	1.169	10	0.134	31.026	75.63	44.08	38.87	41.5	19.87
Solution # 20	24.093	1	9	0.133	31.121	75.24	44.54	36.58	35.83	20.09

AEC: Annual Energy Contribution.

In case when solution #10 is selected by the designer, the power generated by the PV panels is 41.726 kW, the autonomy days is equal to 2.711, and ten wind turbines are required, which generates a total power of 20 kW. This solution corresponds to a COE of 0.187 USD/kW h, an LPSP of 28.424%, and an RF of 85.90%.

If solution #20 is selected by the designer, the total power generated by the PV panels is 24.093 kW, one autonomy day is required, and nine wind turbines are required to generate a total power of 18 kW. This solution corresponds to a COE of 0.133 USD/kW h, an LPSP of 31.121%, and an RF of 75.24%.

The annual contributions of energy generated by each source in the studied power generation system (i.e., PV, WT, BT, and DG) for solutions #1, #10, and #20 of the first algorithm are represented in Figure 13a–c, respectively. The annual contribution of the energy produced by the PV panels is 121.80 MW, which presents 42% of the total generated energy in solution #1 of the first algorithm, shown in Figure 13a and Table 6. It can be clearly observed that this production is higher compared to solution #10 and solution #20. The WT and DG provide 38.87 MW and 15.33 MW, respectively, which represent 13 and 5%, respectively, of the total generated energy in solution #1. It can be clearly noted that is lower than the energy contribution of the WT and DG in solution #10 and solution #20. The BT contributes 118.33 MW, which represents 40% of the total generated energy in solution #1. In Figure 13b, the annual contributions of the energy provided by the PV, WT, BT, and DG are 77.14 MW, 38.87 MW, 102.74 MW, and 16.36 MW, representing 33, 16, 44, and 7% of the total generated energy in solution #10, respectively.

Figure 13c shows the annual contribution of the energy provided by each source—PV, WT, BT, and DG—as 44.54 MW, 36.58 MW, 35.83 MW, and 20.09 MW, which represent 32, 27, 26, and 15% of the total generated energy in solution #20, respectively.

The same analysis can also be made for the results of MODA, MOGOA, and MOALO when the algorithms are changed while maintaining the same system.
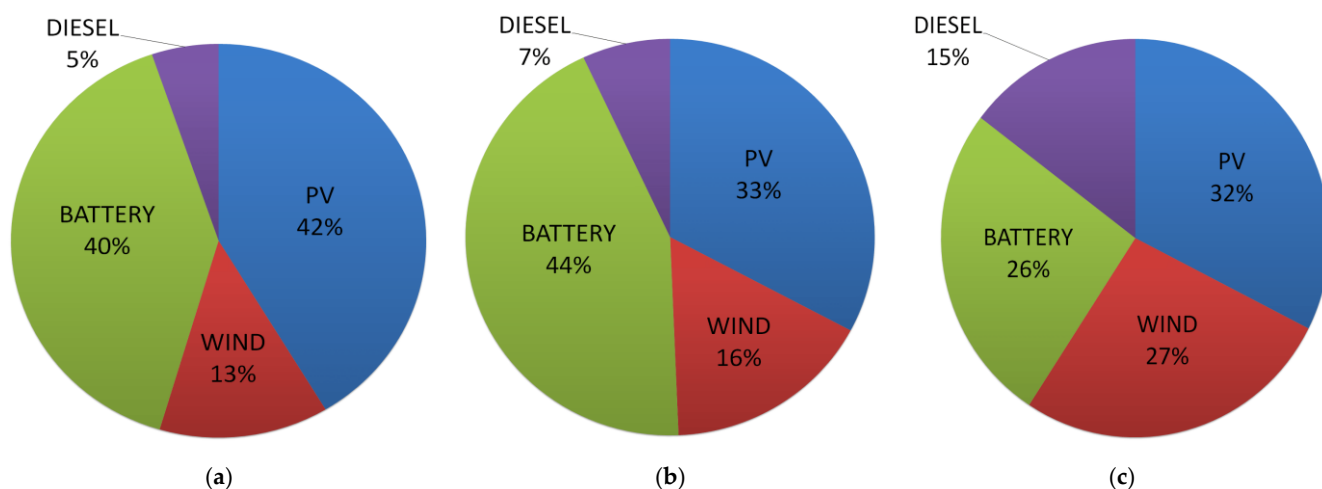
Figure 13. The annual contribution of energy generation by PV/WT/battery and DG for MOSSA.
(**a**) Solution #1; (**b**) solution #10; (**c**) solution #20.

Comparison between MOSSA and the Other Techniques

In this section, the performance of the MOSSA algorithm has been compared to the MODA, MOGOA, and MOALO algorithms for solving the optimization problem investigated in this paper. From the previously obtained results in Figure 12a–d and Tables 6–9, MOSSA provided the best solution (Solution #1, Table 6) among the optimal solutions, corresponding to a COE of 0.255 USD/kW h and an LPSP of 27.079%. MODA, MOGOA, and MOALO algorithms provided more expensive solutions than MOSSA with a COE of 0.286 USD/kW h and an LPSP of 27.149%; a COE of 0.307 USD/kW h and an LPSP of 27.021%; and a COE of 0.290 USD/kW h and an LPSP of 27.018%, respectively. In addition, MOSSS balanced the contributions of renewable energy sources in a way that corresponds to the objective function by a PV of 42%, WT of 13%, batteries of 40%, and DG of 5%. The other contributions of energy generation by PV/WT/battery and DG for MODA, MOGOA, and MOALO are presented in Figures 14–16, respectively. On the other hand, MOGOA provided the best RE result among the previous algorithms, and at the same time, it had the highest COE among them, indicating that it did not succeed in balancing between COE and LPSP.
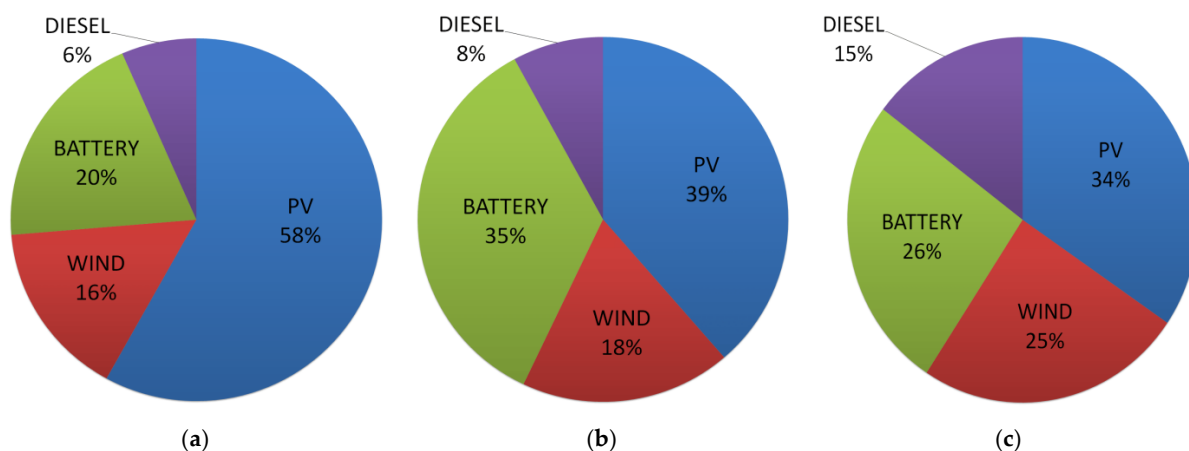

Figure 14. The annual contribution of energy generation by PV/WT/battery and DG for MODA.
(**a**) Solution #1; (**b**) solution #10; (**c**) solution #20.

Table 7. Selected solutions from the Pareto front of MODA.

Solution #	PV (KW)	N^{AD}	N^{WT}	COE (USD/kW h)	LPSP (%)	RE (%)	The AEC from PV (MW)	The AEC from WT (MW)	The AEC from BT (MW)	The AEC from DG (MW)
Solution #1	78.057	1.215	10	0.286	27.149	90.99	144.3	38.87	49.24	16.24
Solution #2	76.811	1.119	10	0.283	27.154	90.99	142	38.87	45.48	16.3
Solution #3	76.499	1.137	10	0.282	27.155	90.96	141.42	38.87	46.15	16.29
Solution #4	75.377	1.478	10	0.28	27.158	90.99	139.35	38.87	59.52	16.07
Solution #5	74.679	1.478	10	0.278	27.177	90.91	138.06	38.87	59.49	16.08
Solution #6	73.399	1.437	10	0.274	27.215	90.76	135.69	38.87	57.8	16.13
Solution #7	73.368	1.452	10	0.274	27.223	90.77	135.63	38.87	58.41	16.11
Solution #8	74.282	1.135	9	0.273	27.642	90.47	137.32	36.65	45.69	16.53
Solution #9	54.734	2.271	10	0.221	28.132	88.41	101.19	38.87	88.25	16.07
Solution #10	44.195	1.926	10	0.193	28.425	86.12	81.7	38.87	74.02	16.74
Solution #11	43.87	1.882	10	0.192	28.495	86.01	81.1	38.87	72.32	16.77
Solution #12	34.075	2.6	10	0.165	29.184	83.16	62.99	38.87	95.47	17.07
Solution #13	33.13	1	10	0.16	29.523	81.51	61.25	38.87	37.85	18.38
Solution #14	29.655	1.342	9	0.149	30.257	79.62	54.82	36.65	48.94	18.64
Solution #15	28.743	1.436	9	0.146	30.482	78.93	53.14	36.65	51.86	18.8
Solution #16	28.717	1.4	9	0.146	30.496	78.9	53.09	36.65	50.59	18.82
Solution #17	28.683	1.47	9	0.146	30.502	78.88	53.03	36.65	53	18.79
Solution #18	28.853	1.383	9	0.144	30.711	78.48	53.34	36.65	49.77	18.98
Solution #19	25.706	1	8	0.134	31.347	75.4	47.52	33.86	35.8	20.08
Solution #20	25.637	1.003	8	0.134	31.411	75.25	47.39	33.86	35.83	20.11

AEC: annual energy contribution.

Table 8. Selected solutions from the Pareto front of MOGOA.

Solution #	PV (KW)	N^{AD}	N^{WT}	COE (USD/kW h)	LPSP (%)	RE (%)	The AEC from PV (MW)	The AEC from WT (MW)	The AEC from BT (MW)	The AEC from DG (MW)
Solution #1	85.825	1.014	10	0.307	27.021	91.74	158.66	38.26	41.47	16.26
Solution #2	74.989	1.007	10	0.277	27.332	90.68	138.63	38.26	40.91	16.47
Solution #3	66.413	2.695	10	0.254	27.442	90.32	122.78	38.26	106.10	15.53
Solution #4	64.188	2.098	10	0.247	27.825	89.81	118.66	38.26	82.63	15.91
Solution #5	64.188	2.098	10	0.247	27.831	89.80	118.66	38.26	82.62	15.91
Solution #6	64.309	2.721	9	0.244	28.119	89.64	118.89	34.06	105.80	15.85
Solution #7	63.919	2.686	9	0.241	28.356	89.43	118.17	34.06	104.17	15.99
Solution #8	50.841	3.000	9	0.208	28.459	87.56	93.99	34.06	114.34	16.03
Solution #9	48.944	2.079	8	0.198	29.275	86.14	90.48	32.20	79.02	17.01
Solution #10	48.446	1.117	8	0.196	29.304	85.55	89.56	32.20	43.23	17.68
Solution #11	43.247	1.130	9	0.184	29.350	84.57	79.95	34.06	43.38	17.69
Solution #12	43.326	1.115	9	0.184	29.387	84.49	80.10	34.06	42.84	17.75
Solution #13	37.080	1.897	9	0.167	29.811	82.92	68.55	34.06	70.51	17.60
Solution #14	26.733	1.005	10	0.143	30.331	77.88	49.42	38.26	36.79	19.39
Solution #15	25.487	1.117	9	0.134	31.378	75.53	47.12	34.06	39.69	19.94
Solution #16	20.161	1.102	9	0.119	32.600	70.42	37.27	34.06	37.51	21.14
Solution #17	16.490	1.131	8	0.105	34.570	63.46	30.48	32.20	36.34	22.50
Solution #18	12.920	2.682	9	0.102	34.950	61.84	23.89	34.06	76.89	22.47
Solution #19	15.144	1.950	7	0.101	35.199	58.41	28.00	27.21	56.98	22.96
Solution #20	12.565	1.242	6	0.084	38.810	45.94	23.23	23.32	34.44	25.17

AEC: annual energy contribution.

As mentioned previously, this work attaches importance to preserving the environment. In this sense, MOSSA provided the lowest fuel consumed by DGs of 15.33 MW annual contribution compared to others, where contribution in MODA was 16.24 MW, contribution in MOGOA was 16.26 MW, and contribution in MOALO was 15.38 MW.

Figure 17 summarizes the comparison results between the previous algorithms; it can be noted clearly that the MOSSA algorithm offers better convergence than others, as it has a broader and consistent distribution in the Pareto front. It can be said that the MOSSA has good performance in improving system cost and reliability, and it provides better COE and LPSP. The obtained results indicate that the proposed MOSSA possesses good performance in solving such types multiobjective problems.

Table 9. Selected solutions from the Pareto front of MOALO.

Solution #	PV (KW)	N^{AD}	N^{WT}	COE (USD/kW h)	LPSP (%)	RE (%)	The AEC from PV (MW)	The AEC from WT (MW)	The AEC from BT (MW)	The AEC from DG (MW)
Solution #1	78.813	2.39	10	0.29	27.018	91.67	145.7	38.87	95.56	15.38
Solution #2	75.317	1.953	10	0.28	27.228	91.19	139.24	38.87	78.09	15.69
Solution #3	64.59	2.666	10	0.251	27.339	90.21	119.41	38.87	105.12	15.49
Solution #4	62.96	1.842	10	0.245	27.54	89.64	116.39	38.87	72.98	16.08
Solution #5	51.387	2.629	10	0.214	27.882	88.13	95	38.87	101.8	15.89
Solution #6	46.735	1.629	10	0.2	28.358	86.56	86.4	38.87	63.15	16.81
Solution #7	42.991	1	10	0.189	28.602	85.19	79.48	38.87	39.15	17.52
Solution #8	38.052	1.555	10	0.174	29.262	83.85	70.35	38.87	58.83	17.43
Solution #9	35.045	1.644	10	0.166	29.414	82.86	64.79	38.87	61.53	17.61
Solution #10	33.112	1.615	10	0.161	29.561	82.08	61.21	38.87	59.93	17.81
Solution #11	29.121	2.008	10	0.151	29.829	80.53	53.84	38.87	72.39	18.05
Solution #12	28.185	1	10	0.147	30.008	79.02	52.11	38.87	37.07	19.09
Solution #13	24.526	1.532	10	0.135	31.072	76.37	45.34	38.87	53.61	19.43
Solution #14	20.076	1.517	10	0.123	32.053	72.44	37.11	38.87	51.13	20.44
Solution #15	15.922	1.535	10	0.112	33.344	67.56	29.43	38.87	49.33	21.57
Solution #16	16.957	1.49	8	0.107	34.326	64.96	31.35	31.53	47.24	22.03
Solution #17	12.117	1.395	9	0.097	35.741	58.93	22.4	34.55	41.29	23.39
Solution #18	12.169	3	8	0.095	36.589	56.12	22.5	31.53	81.18	23.37
Solution #19	12.474	1	7	0.089	37.443	51.31	23.06	27.52	29.39	24.63
Solution #20	13.973	1.103	6	0.087	38.106	49.55	25.83	22.94	31.89	24.61

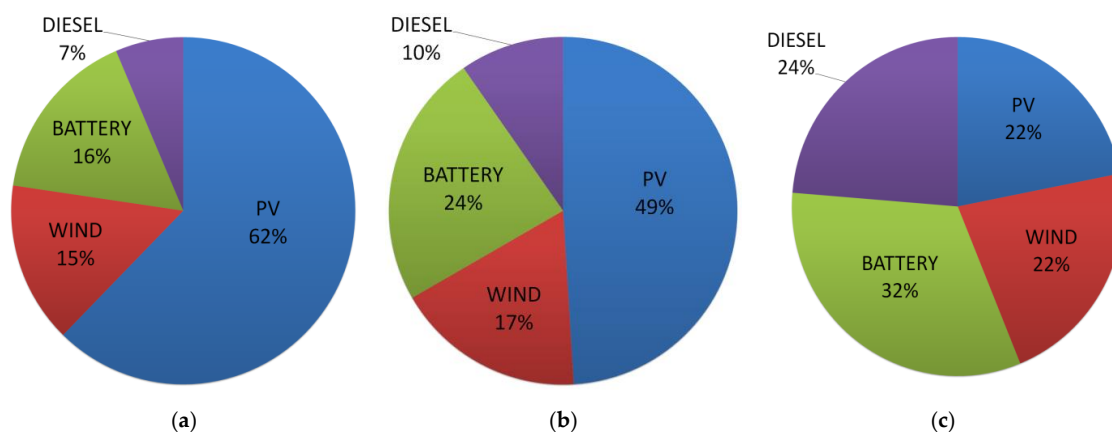AEC: annual energy contribution.

(**a**)   (**b**)   (**c**)

Figure 15. The annual contribution of energy generation by PV/WT/battery and DG for MOGOA. (**a**) Solution #1; (**b**) solution #10; (**c**) solution #20.
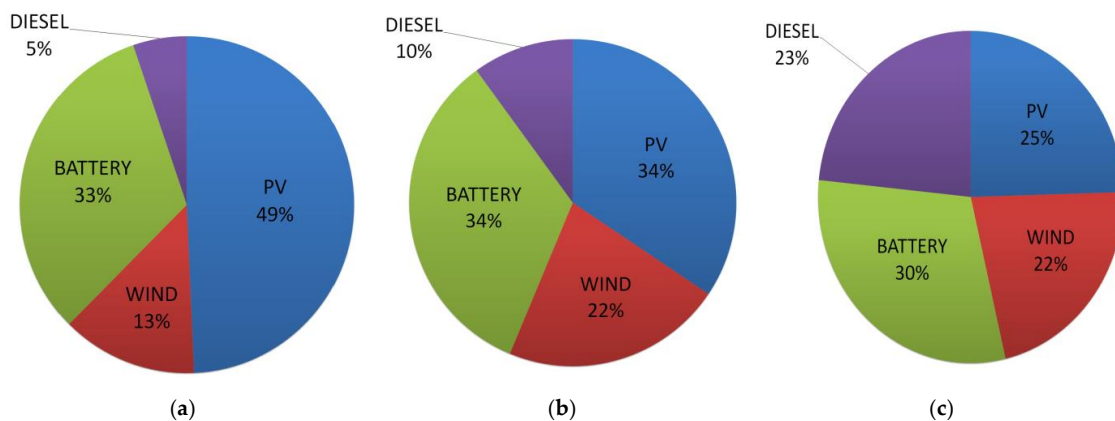

(**a**)   (**b**)   (**c**)

Figure 16. The annual contribution of energy generation by PV/WT/battery and DG for MOALO. (**a**) Solution #1; (**b**) solution #10; (**c**) solution #20.
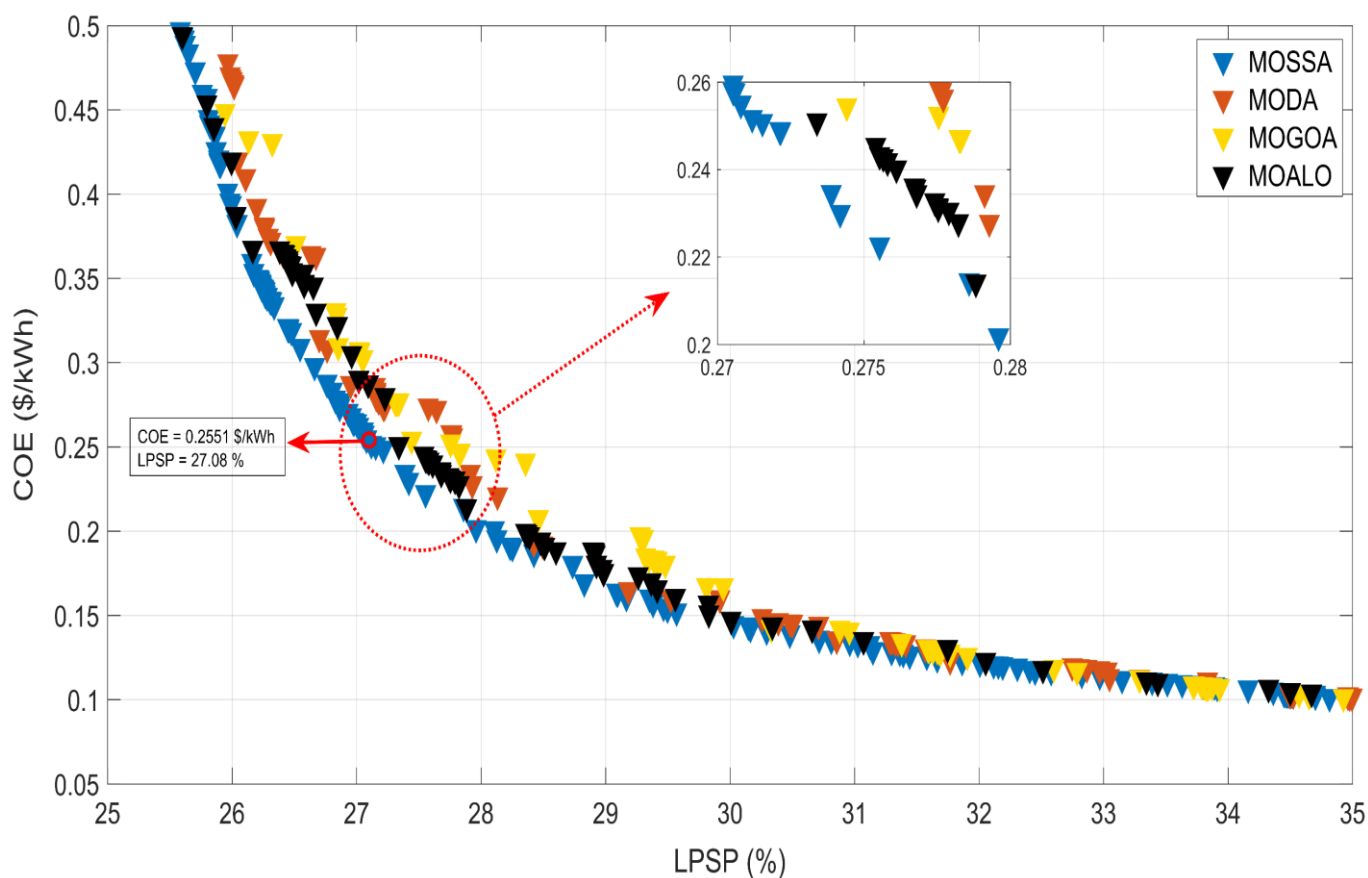
Figure 17. Pareto front of stand-alone microgrid system considering LPSP and COE obtained by MOSSA, MODA, MOGOA, and MOALO.

After comparing the previous algorithms, the solution #1 corresponding to the first algorithm is chosen, which ensures the optimal design of the studied stand-alone microgrid system of HRES consisting of PV/WT/battery and DG system to fulfill the load energy demand as shown in Figure 1. The obtained optimal solution allows ensuring total annual power generations of 121.80 MW, 38.87 MW, 118.33 MW, and 15.33 MW by PV, WT, battery, and DG, respectively, as presented in Table 6.

The annual generated power by the PV and wind turbine according to the selected optimal system configuration are presented in Figure 18a,b, respectively. The contribution of the backup system (diesel generator) is shown in Figure 18c. At the same time, the SOC of the battery is shown in Figure 18d, while Figure 19 presents the total annual power generated by all sources—PV, WT, battery, and DG—and the load power demand.

For example, if the period [8300; 8200] in hours during the winter season is chosen in order to observe the behavior of the SOC of the battery, a zoom is taken from Figure 18d and shown in Figure 20, while Figure 21 shows the contribution of the diesel generator in the same period.
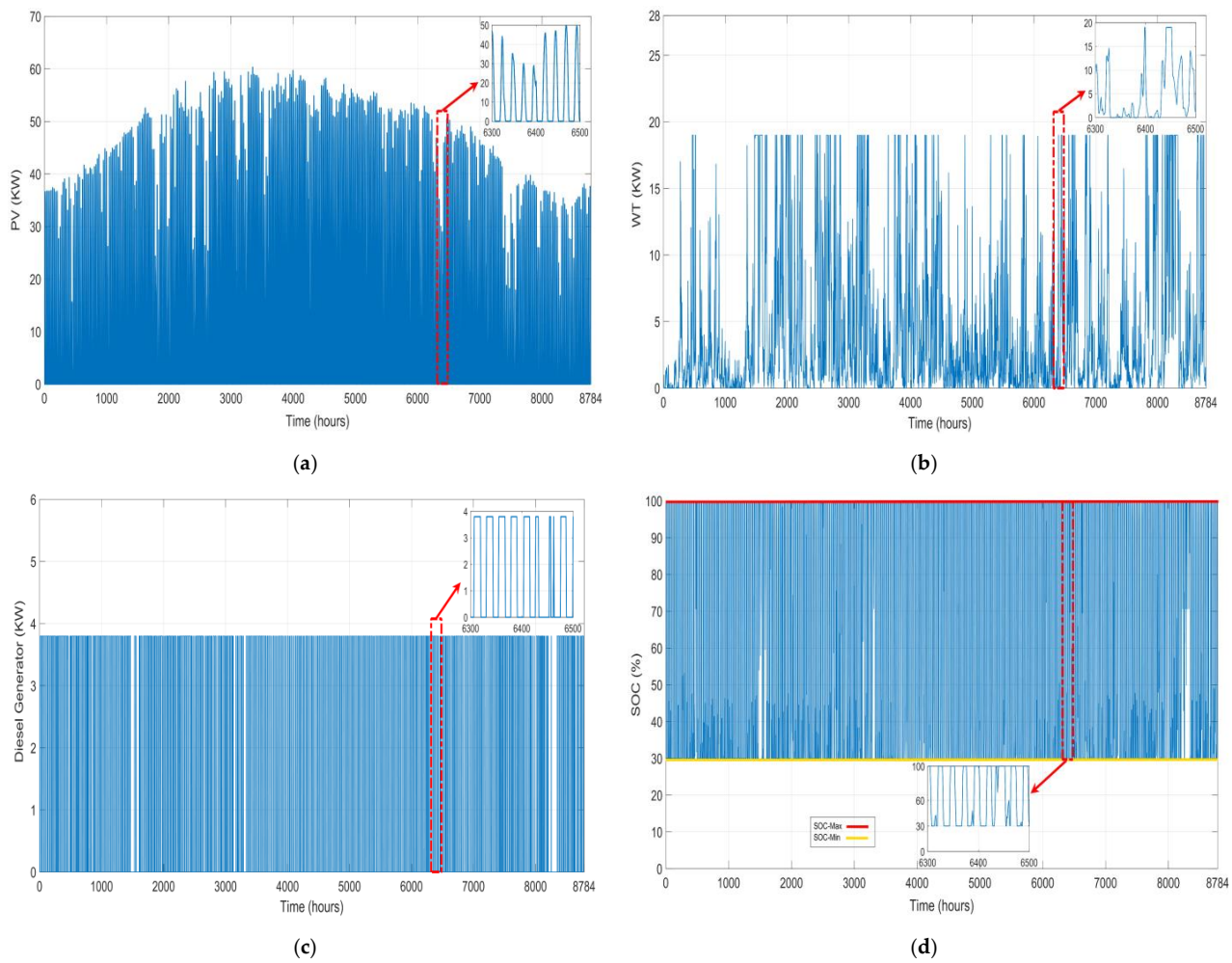
Figure 18. Power generated by the various components of the HMS over one year for MOSSA solution #1. (**a**) PV array; (**b**) WT; (**c**) DG. The annual profile of the battery SOC (**d**).
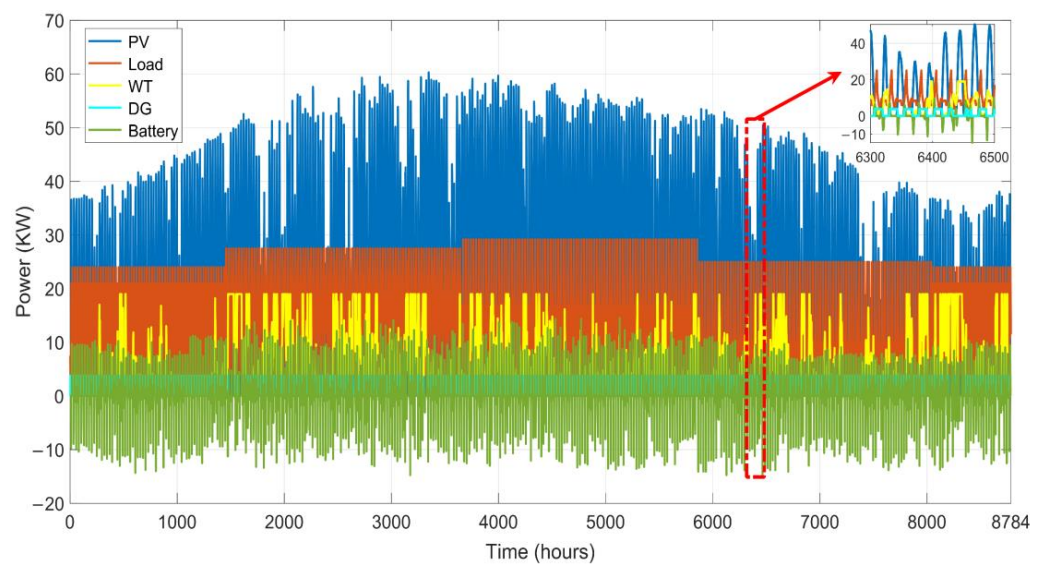

Figure 19. Power generation of the hybrid stand-alone microgrid system over one year.
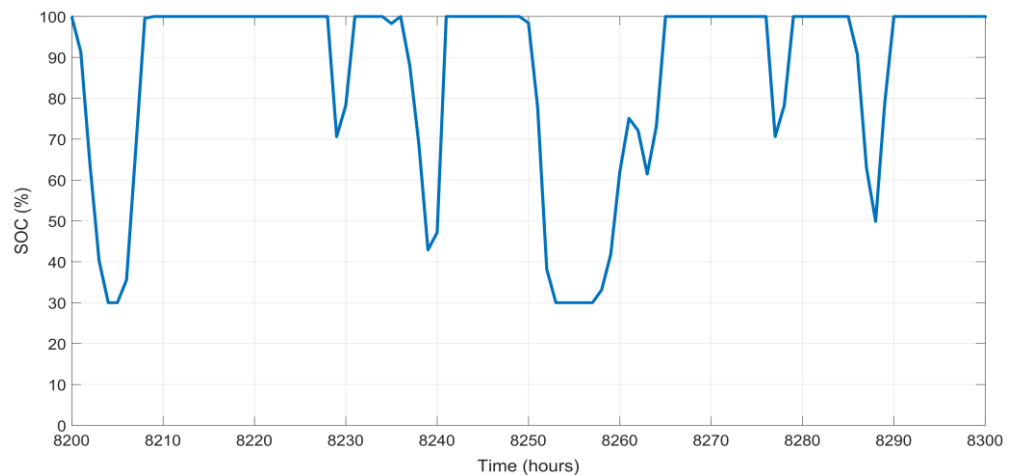
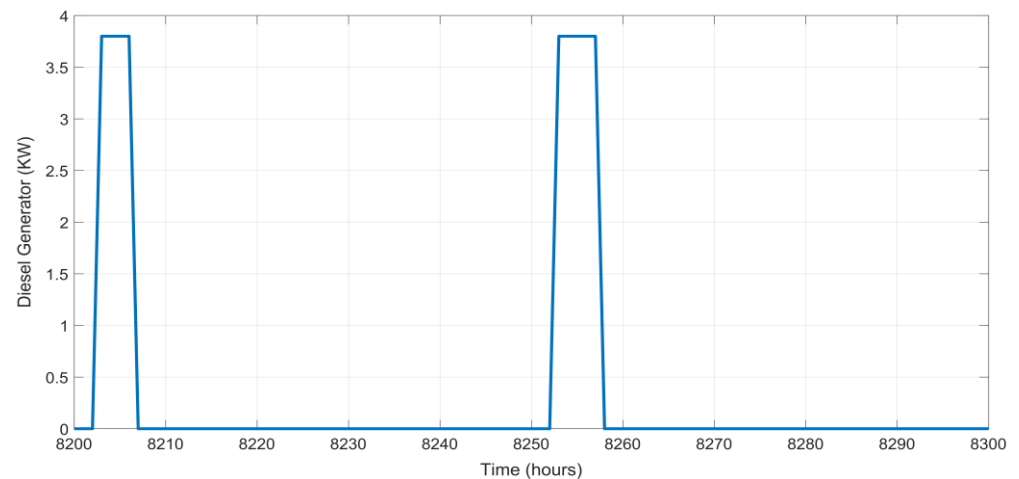**Figure 20.** Hourly variation of the battery SOC during the winter season.

Figure 21. Power generated by DG during winter season.

7. Conclusions

This research paper has proposed an approach for the optimal sizing of a stand-alone microgrid system which is powered by hybrid sources of energy such as PV, WT, BT, and DG and comprises two buses such as a DC bus and an AC bus that are bidirectionally connected with a power electronics conversion system. The main aim of the designed hybrid stand-alone microgrid system is to meet the load energy demand of a remote area in an off-grid community in Djelfa, Algeria. Indeed, this paper has proposed an optimization design based on a recent nature-inspired metaheuristic optimization algorithm called the multiobjective salp swarm algorithm in order to find the minimum cost of electricity COE and minimum potential for electrical loss LPSP at the same time. Moreover, the renewable energy factor has been introduced to ensure that the system works mainly on renewable energy resources. To prove the validity and the effectiveness of the proposed approach using MOSSA, simulations have been carried out based on real data collected from the study site. The obtained results based on MOSSA have been compared with those obtained using MODA, MOGOA, and MOALO and some previously obtained results, where it has been proved that the proposed approach based on MOSSA yields better results; it contributed 90.46% of RF, a COE of 0.255 USD/kW h, and an LPSP of 27.079%. This outperforms MODA, MOGOA, and MOALO, where the offered optimal solutions show clear superiority compared to other presented results due to the design goal of the hybrid stand-alone microgrid system being to obtain a set of solutions to be adopted following different scenarios which can be faced in real cases. Finally, it can be concluded that the

proposed approach based on the MOSSA can be a promising tool for the designer to obtain optimal design solutions.

As part of future work, other renewable energy sources can be added and diversified in line with the capabilities of each region. The newly discovered artificial intelligence algorithms can also be applied. Another perspective is the study of optimal sizing using hybrid optimization techniques for further explorations in future research and facing the complexities and challenges of hybrid systems.

Author Contributions: Conceptualization, Z.B., A.K., B.T., L.M. and A.B.; methodology, Z.B., A.K. and B.T.; validation, Z.B., A.K. and B.T.; formal analysis, Z.B., A.K., B.T., L.M., A.B. and M.A.; investigation, A.K., L.M. and M.A.; resources, A.K., B.T., L.M. and A.B.; data curation, Z.B.; writing—original draft preparation, Z.B.; writing—review and editing, A.K., B.T., L.M., R.K. and M.A.; visualization, Z.B., B.T. and A.K.; supervision, A.K.; project administration, A.K.; funding acquisition, R.K. and M.A. All authors have read and agreed to the published version of the manuscript.

Institutional Review Board Statement: Not Applicable.

Informed Consent Statement: Not Applicable.

Data Availability Statement: Wind speed, solar radiation, and ambient temperature data presented in this study are openly available at http://www.soda-pro.com/web-services/meteodata, accessed on 6 October 2021. The other data presented in this study are available in the body of this paper.

Conflicts of Interest: The authors declare no conflict of interest.

References

1.　Dalton, G.J.; Lockington, D.A.; Baldock, T.E. Case study feasibility analysis of renewable energy supply options for small to medium-sized tourist accommodations. *Renew. Energy* **2009**, *34*, 1134–1144. [CrossRef]
2.　Kaldellis, J.K.; Zafirakis, D. The wind energy (r)evolution: A short review of a long history. *Renew. Energy* **2011**, *36*, 1887–1901. [CrossRef]
3.　Fathabadi, H. Novel grid-connected solar/wind powered electric vehicle charging station with vehicle-to-grid technology. *Energy* **2017**, *132*, 1–11. [CrossRef]
4.　Ghorbani, N.; Kasaeian, A.; Toopshekan, A.; Bahrami, L.; Maghami, A. Optimizing a hybrid wind-PV-battery system using GA-PSO and MOPSO for reducing cost and increasing reliability. *Energy* **2018**, *154*, 581–591. [CrossRef]
5.　United Nations Development Programme (UNDP). UNDP and Energy Access for the Poor: Energizing the Millennium Development Goals. In *Environment & Energy, United Nations Development Programme*; UNDP: New York, NY, USA, 2011.
6.　Borhanazad, H.; Mekhilef, S.; Gounder Ganapathy, V.; Modiri-Delshad, M.; Mirtaheri, A. Optimization of micro-grid system using MOPSO. *Renew. Energy* **2014**, *71*, 295–306. [CrossRef]
7.　Celik, A.N. Techno-economic analysis of autonomous PV-wind hybrid energy systems using different sizing methods. *Energy Convers. Manag.* **2003**, *44*, 1951–1968. [CrossRef]
8.　Dufo-López, R.; Bernal-Agustín, J.L. Design and control strategies of PV-diesel systems using genetic algorithms. *Sol. Energy* **2005**, *79*, 33–46. [CrossRef]
9.　Wiemann, M.; Rolland, S.; Glania, G. Hybrid Mini-Grids for Rural Electrification: Lessons Learned. In Proceedings of the Region 10 Conference (TENCON), Singapore, 22–25 November 2016; pp. 1270–1273.
10.　Bukar, A.L.; Modu, B.; Gwoma, Z.M.; Mustapha, M.; Buji, A.B.; Lawan, M.B.; Tijjani, I.; Benisheik, U.A.; Bukar, A.; Mai, K.B. Economic Assessment of a PV/Diesel/Battery Hybrid Energy System for a Non-Electrified Remote Village in Nigeria. *Eur. J. Eng. Res. Sci.* **2017**, *2*, 21. [CrossRef]
11.　Bukar, A.L.; Tan, C.W.; Lau, K.Y. Optimal sizing of an autonomous photovoltaic/wind/battery/diesel generator microgrid using grasshopper optimization algorithm. *Sol. Energy* **2019**, *188*, 685–696. [CrossRef]
12.　Nadjemi, O.; Nacer, T.; Hamidat, A.; Salhi, H. Optimal hybrid PV/wind energy system sizing: Application of cuckoo search algorithm for Algerian dairy farms. *Renew. Sustain. Energy Rev.* **2017**, *70*, 1352–1365. [CrossRef]
13.　Al-falahi, M.D.A.; Jayasinghe, S.D.G.; Enshaei, H. A review on recent size optimization methodologies for standalone solar and wind hybrid renewable energy system. *Energy Convers. Manag.* **2017**, *143*, 252–274. [CrossRef]
14.　Khatib, T.; Ibrahim, I.A.; Mohamed, A. A review on sizing methodologies of photovoltaic array and storage battery in a standalone photovoltaic system. *Energy Convers. Manag.* **2016**, *120*, 430–448. [CrossRef]

15. Sinha, S.; Chandel, S.S. Review of recent trends in optimization techniques for solar photovoltaic-wind based hybrid energy systems. *Renew. Sustain. Energy Rev.* **2015**, *50*, 755–769. [CrossRef]

16. Anoune, K.; Bouya, M.; Astito, A.; Abdellah, A. Ben Sizing methods and optimization techniques for PV-wind based hybrid renewable energy system: A review. *Renew. Sustain. Energy Rev.* **2018**, *93*, 652–673. [CrossRef]

17. Bashir, N.; Modu, B. Techno-economic analysis of off-grid renewable energy systems for rural electrification in Northeastern Nigeria. *Int. J. Renew. Energy Res.* **2018**, *8*, 1217–1228.

18. Ajlan, A.; Tan, C.W.; Abdilahi, A.M. Assessment of environmental and economic perspectives for renewable-based hybrid power system in Yemen. *Renew. Sustain. Energy Rev.* **2017**, *75*, 559–570. [CrossRef]

19. Sinha, S.; Chandel, S.S. Review of software tools for hybrid renewable energy systems. *Renew. Sustain. Energy Rev.* **2014**, *32*, 192–205. [CrossRef]

20. Bernal-Agustín, J.L.; Dufo-López, R. Simulation and optimization of stand-alone hybrid renewable energy systems. *Renew. Sustain. Energy Rev.* **2009**, *13*, 2111–2118. [CrossRef]

21. Al Garni, H.Z.; Abubakar Mas'ud, A.; Wright, D. Design and economic assessment of alternative renewable energy systems using capital cost projections: A case study for Saudi Arabia. *Sustain. Energy Technol. Assess.* **2021**, *48*, 101675. [CrossRef]

22. Seedahmed, M.M.A.; Ramli, M.A.M.; Bouchekara, H.R.E.H.; Milyani, A.H.; Rawa, M.; Nur Budiman, F.; Firmansyah Muktiadji, R.; Mahboob Ul Hassan, S. Optimal sizing of grid-connected photovoltaic system for a large commercial load in Saudi Arabia. *Alex. Eng. J.* **2022**, *61*, 6523–6540. [CrossRef]

23. Thirunavukkarasu, M.; Sawle, Y. A Comparative Study of the Optimal Sizing and Management of Off-Grid Solar/Wind/Diesel and Battery Energy Systems for Remote Areas. *Front. Energy Res.* **2021**, *9*, 752043. [CrossRef]

24. Tozzi, P.; Jo, J.H. A comparative analysis of renewable energy simulation tools: Performance simulation model vs. system optimization. *Renew. Sustain. Energy Rev.* **2017**, *80*, 390–398. [CrossRef]

25. Kazem, H.A.; Khatib, T.; Sopian, K. Sizing of a standalone photovoltaic/battery system at minimum cost for remote housing electrification in Sohar, Oman. *Energy Build.* **2013**, *61*, 108–115. [CrossRef]

26. Ayop, R.; Isa, N.M.; Tan, C.W. Components sizing of photovoltaic stand-alone system based on loss of power supply probability. *Renew. Sustain. Energy Rev.* **2018**, *81*, 2731–2743. [CrossRef]

27. Abdul Aziz, N.I.; Sulaiman, S.I.; Shaari, S.; Musirin, I.; Sopian, K. Optimal sizing of stand-alone photovoltaic system by minimizing the loss of power supply probability. *Sol. Energy* **2017**, *150*, 220–228. [CrossRef]

28. Sanajaoba, S.; Fernandez, E. Maiden application of Cuckoo Search algorithm for optimal sizing of a remote hybrid renewable energy System. *Renew. Energy* **2016**, *96*, 1–10. [CrossRef]

29. Zhang, X.; Tan, S.C.; Li, G.; Li, J.; Feng, Z. Components sizing of hybrid energy systems via the optimization of power dispatch simulations. *Energy* **2013**, *52*, 165–172. [CrossRef]

30. Khatod, D.K.; Pant, V.; Sharma, J. Analytical approach for well-being assessment of small autonomous power systems with solar and wind energy sources. *IEEE Trans. Energy Convers.* **2010**, *25*, 535–545. [CrossRef]

31. Lujano-Rojas, J.M.; Dufo-López, R.; Bernal-Agustín, J.L. Probabilistic modelling and analysis of stand-alone hybrid power systems. *Energy* **2013**, *63*, 19–27. [CrossRef]

32. Fathy, A.; Kaaniche, K.; Alanazi, T.M. Recent Approach Based Social Spider Optimizer for Optimal Sizing of Hybrid PV/Wind/Battery/Diesel Integrated Microgrid in Aljouf Region. *IEEE Access* **2020**, *8*, 57630–57645. [CrossRef]

33. Farh, H.M.H.; Al-Shamma, A.A.; Al-shaalan, A.M.; Alkuhayli, A. Technical and Economic Evaluation for Off-Grid Hybrid Renewable Energy System Using Novel Bonobo Optimizer. *Sustainability* **2022**, *14*, 1533. [CrossRef]

34. Jufri, F.H.; Aryani, D.R.; Garniwa, I.; Sudiarto, B. Optimal battery energy storage dispatch strategy for small-scale isolated hybrid renewable energy system with different load profile patterns. *Energies* **2021**, *14*, 3139. [CrossRef]

35. Ramli, M.A.M.; Bouchekara, H.R.E.H.; Alghamdi, A.S. Optimal sizing of PV/wind/diesel hybrid microgrid system using multi-objective self-adaptive differential evolution algorithm. *Renew. Energy* **2018**, *121*, 400–411. [CrossRef]

36. Bouchekara, H.R.E.H.; Javaid, M.S.; Shaaban, Y.A.; Shahriar, M.S.; Ramli, M.A.M.; Latreche, Y. Decomposition based multiobjective evolutionary algorithm for PV/Wind/Diesel Hybrid Microgrid System design considering load uncertainty. *Energy Rep.* **2021**, *7*, 52–69. [CrossRef]

37. Bukar, A.L.; Tan, C.W.; Yiew, L.K.; Ayop, R.; Tan, W.S. A rule-based energy management scheme for long-term optimal capacity planning of grid-independent microgrid optimized by multi-objective grasshopper optimization algorithm. *Energy Convers. Manag.* **2020**, *221*, 113161. [CrossRef]

38. Omar, A.S. Multi-Objective Optimization of a Stand-alone Hybrid PV/wind/battery/diesel Micro-grid. In Proceedings of the IEEE Conference on Power Electronics and Renewable Energy, CPERE 2019, Aswan, Egypt, 23–25 October 2019; pp. 391–396.

39. Bouchekara, H.R.E.H.; Shahriar, M.S.; Irshad, U.B.; Sha'aban, Y.A.; Mahmud, M.A.P.; Javaid, M.S.; Ramli, M.A.M.; Farjana, S.H. Optimal sizing of hybrid photovoltaic/diesel/battery nanogrid using a parallel multiobjective PSO-based approach: Application to desert camping in Hafr Al-Batin city in Saudi Arabia. *Energy Rep.* **2021**, *7*, 4360–4375. [CrossRef]

40. Zhu, W.; Guo, J.; Zhao, G.; Zeng, B. Optimal sizing of an island hybrid microgrid based on improved multi-objective grey wolf optimizer. *Processes* **2020**, *8*, 1581. [CrossRef]

41. Fathy, A. Reliable and efficient approach for mitigating the shading effect onphotovoltaic module based on Modified Artificial Bee Colony algorithm. *Renew. Energy* **2015**, *81*, 78–88. [CrossRef]

42. Ayop, R.; Tan, C.W. A comprehensive review on photovoltaic emulator. *Renew. Sustain. Energy Rev.* **2017**, *80*, 430–452. [CrossRef]

43. Huld, T.; Gottschalg, R.; Beyer, H.G.; Topič, M. Mapping the performance of PV modules, effects of module type and data averaging. *Sol. Energy* **2010**, *84*, 324–338. [CrossRef]

44. Daud, A.K.; Ismail, M.S. Design of isolated hybrid systems minimizing costs and pollutant emissions. *Renew. Energy* **2012**, *44*, 215–224. [CrossRef]

45. Hamrouni, N.; Jraidi, M. Chérif, a Solar radiation and ambient temperature effects on the performances of a PV pumping system. *Rev. Energ. Renouvelables* **2008**, *11*, 95–106.

46. Sukamongkol, Y.; Chungpaibulpatana, S.; Ongsakul, W. A simulation model for predicting the performance of a solar photovoltaic system with alternating current loads. *Renew. Energy* **2002**, *27*, 237–258. [CrossRef]

47. Wang, L.; Tan, A.C.C.; Cholette, M.; Gu, Y. Comparison of the effectiveness of analytical wake models for wind farm with constant and variable hub heights. *Energy Convers. Manag.* **2016**, *124*, 189–202. [CrossRef]

48. Justus, C.G. Wind energy statistics for large arrays of wind turbines (New England and Central U.S. Regions). *Sol. Energy* **1978**, *20*, 379–386. [CrossRef]

49. Rehman, S.; Al-Abbadi, N.M. Wind shear coefficients and energy yield for Dhahran, Saudi Arabia. *Renew. Energy* **2007**, *32*, 738–749. [CrossRef]

50. Jaramillo, O.A.; Borja, M.A. Wind speed analysis in La Ventosa, Mexico: A bimodal probability distribution case. *Renew. Energy* **2004**, *29*, 1613–1630. [CrossRef]

51. Farrugia, R.N. The wind shear exponent in a Mediterranean island climate. *Renew. Energy* **2003**, *28*, 647–653. [CrossRef]

52. IES 2005 Wind Turbines-Part 1: Design Requirements. In *International Standard*; International Electrotechnical Commission: 2005; Volume 2005, p. 88. Available online: https://www.iec.ch/dyn/www/f?p=103:7:508880294409522::::FSP_ORG_ID:1282 (accessed on 6 April 2022).

53. Patel, M.R. *Book Review: Wind and Solar Power Systems—Design, Analysis, and Operation*; CRC Press: Boca Raton, FL, USA, 2006; Volume 30, ISBN 0849316057.

54. Wang, L.; Singh, C. PSO-based multi-criteria optimum design of a grid-connected hybrid power system with multiple renewable sources of energy. In Proceedings of the 2007 IEEE Swarm Intelligence Symposium, SIS 2007, Honolulu, HI, USA, 1–5 April 2007; pp. 250–257. [CrossRef]

55. Guangqian, D.; Bekhrad, K.; Azarikhah, P.; Maleki, A. A hybrid algorithm based optimization on modeling of grid independent biodiesel-based hybrid solar/wind systems. *Renew. Energy* **2018**, *122*, 551–560. [CrossRef]

56. Kharrich, M.; Kamel, S.; Alghamdi, A.S.; Eid, A.; Mosaad, M.I.; Akherraz, M.; Abdel-Akher, M. Optimal design of an isolated hybrid microgrid for enhanced deployment of renewable energy sources in Saudi Arabia. *Sustainability* **2021**, *13*, 4708. [CrossRef]

57. Mahmoud, M.M.; Ibrik, I.H. Techno-economic feasibility of energy supply of remote villages in Palestine by PV-systems, diesel generators and electric grid. *Renew. Sustain. Energy Rev.* **2006**, *10*, 128–138. [CrossRef]

58. Jayachandran, M.; Ravi, G. Design and Optimization of Hybrid Micro-Grid System. *Energy Procedia* **2017**, *117*, 95–103. [CrossRef]

59. Satish Kumar Ramoji, B.J.K. Optimal Economical Sizing of A PV-Wind Hybrid Energy System Using Genetic Algorithm and Teaching Learning Based Optimization. *Int. J. Green Energy* **2011**, *8*, 25–43.

60. Hatata, A.Y.; Osman, G.; Aladl, M.M. An optimization method for sizing a solar/wind/battery hybrid power system based on the artificial immune system. *Sustain. Energy Technol. Assess.* **2018**, *27*, 83–93. [CrossRef]

61. Skarstein, O.; Uhlen, K. Design considerations with respect to long-term diesel saving in wind/diesel plants. *Wind Eng.* **1989**, *13*, 72–87.

62. Azoumah, Y.; Yamegueu, D.; Ginies, P.; Coulibaly, Y.; Girard, P. Sustainable electricity generation for rural and peri-urban populations of sub-Saharan Africa: The "flexy-energy" concept. *Energy Policy* **2011**, *39*, 131–141. [CrossRef]

63. Deshmukh, M.K.; Deshmukh, S.S. Modeling of hybrid renewable energy systems. *Renew. Sustain. Energy Rev.* **2008**, *12*, 235–249. [CrossRef]

64. Diaf, S.; Diaf, D.; Belhamel, M.; Haddadi, M.; Louche, A. A methodology for optimal sizing of autonomous hybrid PV/wind system. *Energy Policy* **2007**, *35*, 5708–5718. [CrossRef]

65. Darras, C.; Sailler, S.; Thibault, C.; Muselli, M.; Poggi, P.; Hoguet, J.C.; Melscoet, S.; Pinton, E.; Grehant, S.; Gailly, F.; et al. Sizing of photovoltaic system coupled with hydrogen/oxygen storage based on the ORIENTE model. *Int. J. Hydrogen Energy* **2010**, *35*, 3322–3332. [CrossRef]

66. MERRA-2 Re-Analysis. WEB SERVICES—SODA. Available online: http://www.soda-pro.com/web-services/meteodata (accessed on 6 October 2021).

67. Yang, H.; Zhou, W.; Lu, L.; Fang, Z. Optimal sizing method for stand-alone hybrid solar-wind system with LPSP technology by using genetic algorithm. *Sol. Energy* **2008**, *82*, 354–367. [CrossRef]

68. Rajkumar, R.K.; Ramachandaramurthy, V.K.; Yong, B.L.; Chia, D.B. Techno-economical optimization of hybrid pv/wind/battery system using Neuro-Fuzzy. *Energy* **2011**, *36*, 5148–5153. [CrossRef]

69. Kaabeche, A.; Belhamel, M.; Ibtiouen, R. Techno-economic valuation and optimization of integrated photovoltaic/wind energy conversion system. *Sol. Energy* **2011**, *85*, 2407–2420. [CrossRef]

70. Fathy, A. A reliable methodology based on mine blast optimization algorithm for optimal sizing of hybrid PV-wind-FC system for remote area in Egypt. *Renew. Energy* **2016**, *95*, 367–380. [CrossRef]

71. Kashefi Kaviani, A.; Riahy, G.H.; Kouhsari, S.M. Optimal design of a reliable hydrogen-based stand-alone wind/PV generating system, considering component outages. *Renew. Energy* **2009**, *34*, 2380–2390. [CrossRef]

72. Mirjalili, S.; Gandomi, A.H.; Mirjalili, S.Z.; Saremi, S.; Faris, H.; Mirjalili, S.M. Salp Swarm Algorithm: A bio-inspired optimizer for engineering design problems. *Adv. Eng. Softw.* **2017**, *114*, 163–191. [CrossRef]

73. Aljarah, I.; Habib, M.; Faris, H.; Al-Madi, N.; Heidari, A.A.; Mafarja, M.; Elaziz, M.A.; Mirjalili, S. A dynamic locality multi-objective salp swarm algorithm for feature selection. *Comput. Ind. Eng.* **2020**, *147*, 106628. [CrossRef]

74. Ibrahim, A.; Mohammed, S.; Ali, H.A.; Hussein, S.E. Breast Cancer Segmentation from Thermal Images Based on Chaotic Salp Swarm Algorithm. *IEEE Access* **2020**, *8*, 122121–122134. [CrossRef]

75. Lasmari, A.; Zellagui, M.; El-sehiemy, R.A.; Chenni, R. Multi-objective salp swarm algorithm for performance enhancement of electrical distribution system including DG and DSTATCOM simultaneously. In Proceedings of the 4th International Conference on Artificial Intelligence in Renewable Energetic Systems (IC-AIRES), Tipasa, Algeria, 22–24 November 2020.

76. Shaheen, A.M.; El-Sehiemy, R.A. A Multiobjective Salp Optimization Algorithm for Techno-Economic-Based Performance Enhancement of Distribution Networks. *IEEE Syst. J.* **2021**, *15*, 1458–1466. [CrossRef]

77. El Sehiemy, R.A.; Selim, F.; Bentouati, B.; Abido, M.A. A novel multi-objective hybrid particle swarm and salp optimization algorithm for technical-economical-environmental operation in power systems. *Energy* **2020**, *193*, 116817. [CrossRef]

78. Wang, J.; Gao, Y.; Chen, X. A novel hybrid interval prediction approach based on modified lower upper bound estimation in combination with multi-objective salp swarm algorithm for short-term load forecasting. *Energies* **2018**, *11*, 1561. [CrossRef]

79. Mirjalili, S. Dragonfly algorithm: A new meta-heuristic optimization technique for solving single-objective, discrete, and multi-objective problems. *Neural Comput. Appl.* **2016**, *27*, 1053–1073. [CrossRef]

80. Mirjalili, S.Z.; Mirjalili, S.; Saremi, S.; Faris, H.; Aljarah, I. Grasshopper optimization algorithm for multi-objective optimization problems. *Appl. Intell.* **2018**, *48*, 805–820. [CrossRef]

81. Mirjalili, S.; Jangir, P.; Saremi, S. Multi-objective ant lion optimizer: A multi-objective optimization algorithm for solving engineering problems. *Appl. Intell.* **2017**, *46*, 79–95. [CrossRef]